R. Hu

A Guide to Basic Pulse-Radar
Maximum-Range Calculation

Part 2 - Derivations of Equations, Bases of Graphs, and Additional Explanations

L. V. BLAKE

Radar Geophysics Branch
Radar Division

December 31, 1969

20040707010

NAVAL RESEARCH LABORATORY
Washington, D.C.

CONTENTS

i

ABSTRACT

A previous report, designated Part 1, with the same main title, presented information of a practical nature, with little or no proofs, derivations of equations, or explanations, except that sources of information not originated by the author were cited, if previously published. This report, Part 2, presents the proofs, derivations, and explanations omitted in Part 1, together with some results which were either previously unpublished or are now out of print. The basic topics covered are probability of detection of a radar signal, calculation of the radar pattern-propagation factor, atmospheric losses, antenna noise temperature, and the relationship of range-prediction errors to the individual errors in the range-equation factors.

PROBLEM STATUS

A GUIDE TO BASIC PULSE-RADAR MAXIMUM-RANGE CALCULATION

PART 2 – DERIVATIONS OF EQUATIONS, BASES OF GRAPHS, AND ADDITIONAL EXPLANATIONS

1. INTRODUCTION

Part 1 has presented, with a minimum of explanation, the equations, definitions, and data required for calculating the maximum range of a pulse radar. In Part 2, the derivations of these equations will be given. The equations and methods used for plotting various curves presented in Part 1 will also be given, and additional explantions of some matters will be furnished.*

2. DERIVATION OF THE RADAR TRANSMISSION EQUATION

The derivation of Eq. (1), Part 1, the radar transmission equation, is given by Kerr (1). The derivation is repeated here in very brief fashion, because of its fundamental importance to the subject of this report.

It is first supposed that a radar transmitting antenna radiates isotropically — that is, with an equal intensity in all directions of space. Then, over the surface of an imaginary transparent sphere surrounding the antenna, which is located at the center of the sphere, assuming a lossless propagation medium, the power density (power flowing through a unit area of the spherical surface) is, by invoking the principle of conservation of energy,

$$S_t = \frac{P_t}{4\pi R^2} \, , \tag{1}$$

where P_t is the total power radiated and R is the radius of the sphere. (Its total surface area is $4\pi R^2$.)

If a target at range R from the transmitting antenna intercepts an amount of power contained in an area σ square meters, and reradiates it isotropically, the reradiated power density returned to the radar antenna will be

$$S_r = \frac{S_t \, \sigma}{4\pi R^2} \tag{2}$$

or, substituting for S_t the right-hand side of Eq. (1),

$$S_r = \frac{P_t \, \sigma}{(4\pi)^2 R^4} \, . \tag{2a}$$

---

*Part 1 is NRL Report 6930, dated Dec. 23, 1969. Its subtitle is "Equations, Definitions, and Aids to Calculation."

An actual target does not, of course, reradiate isotropically; but the standard *definition** of radar cross section is based on Eq. (2); that is,

$$\sigma = \frac{4\pi R^2 S_r}{S_t} .$$

(3)

In other words, if a target at range R is illuminated with a power density S_t watts per square meter *and it returns to the radar antenna* a power density S_r, its radar cross section is given by Eq. (3). (Free-space propagation conditions are here assumed.) Thus the "radar cross section" is an *"equivalent isotropically-reradiating cross section."*

If the radar transmitting antenna has a power gain G_t, in the direction of the target, S_t is increased by the factor G_t; that is, Eq. (2a) becomes

$$S_r = \frac{P_t G_t \sigma}{(4\pi)^2 R^4} .$$

(4)

The receiving "capture area" of an antenna of gain G_r is

$$A_c = \frac{G_r \lambda^2}{4\pi} .$$

(5)

(Thus, the capture area of an isotropic antenna $(G = 1)$ is $\lambda^2/4\pi$.) The *power* delivered to a receiver by a lossless receiving antenna of capture area A_c is, by definition of A_c,

$$P_r = S_r A_c .$$

(6)

Making the substitutions of Eqs. (4) and (5) in Eq. (6) gives

$$P_r = \frac{P_t G_t G_r \sigma \lambda^2}{(4\pi)^3 R^4} .$$

(7)

This is the radar transmission equation for a radar and target located in free space. In the actual earth environment, S_t and S_r are further modified by various propagation effects, such as refraction, diffraction (shadowing), multipath interference, and absorption. If S_r' and S_t' are the values observed in the actual environment, *propagation factors* can be defined such that

$$F_t^2 = S_t'/S_t$$

(8a)

and

$$F_r^2 = S_r'/S_r .$$

(8b)

(Actually, a propagation factor F is basically defined in terms of the ratio of the electric field intensity observed in the actual environment to that in empty space; therefore, F^2 applies to the ratios of the power densities.) The resulting radar transmission equation (expressed in terms of the ratio P_r/P_t) is

---

*The word "definition" is in italics to emphasize the fact that the physical unreality of the isotropic-reradiation assumption is not objectionable, since definitions are to a large extent arbitrary. The only requirement on them is that all subsequent uses of defined terms must be consistent with the definitions. Additional italics in the paragraph have similar motivation.

$$\frac{P_r}{P_t} = \frac{G_t \, G_r \, \sigma \, \lambda^2 \, F_t{}^2 F_r{}^2}{(4\pi)^3 \, R^4} \, . \tag{9}$$

This completes the derivation. (The equation is given by Kerr for a monostatic radar using the same antenna for transmitting and receiving.) However, thus far G_t and G_r have been assumed to be antenna gains in the direction of the target. If, following Kerr, they are defined as gains in the beam-maximum directions, then the reduction of gain, if any, in the target direction is accounted for by additional factors in F_t and F_r. These factors are then called pattern-propagation factors. It has been shown in Part 1 how this basic equation can be elaborated to obtain radar maximum range equations in terms of more readily known quantities, and for more complicated situations.

3. SIGNAL-TO-NOISE RATIO, PROBABILITY OF DETECTION, AND RELATED SUBJECTS

Single-Pulse Detection

The curves of Figs. 4 through 7 of Part 1 were machine computed by the author (and machine plotted), using mathematical results derived by others (with minor exceptions).*

In Part 1 it was explained that the probability of detection is formally given by the expression

$$P_d = \int_{v_t}^{\infty} p_{sn}(v) \, dv \, , \tag{10}$$

where v is the receiver output voltage (after all predecision processing, including integration or averaging of successive pulses in the case of pulse radar, doppler filtering in the case of CW or pulse-doppler radar, etc.) The quantity v_t is a fixed threshold level of voltage that depends (as will be described) on the allowable rate of "false alarms" (decision that a signal is present when in fact there is no signal). The function p_{sn} is the probability density of v, which is a random variable because it is the resultant receiver output when both signal (s) and noise (n) are present in the input.

The probability of a false alarm is

$$P_{fa} = \int_{v_t}^{\infty} p_n(v) \, dv \tag{11}$$

where $p_n(v)$ is the probability density of the detector output voltage when the input is noise, with no signal present. The function p_{sn} must of course reduce to p_n when the signal power has zero value.

The value of P_d, Eq. (10), obviously depends on the value selected for v_t; this value is chosen, as is evident from Eq. (11), by first deciding what value of P_{fa} is desired, or required, and then solving Eq. (11) for the value of v_t that results in this value of P_{fa}. Of course, this solution can be obtained analytically only if $p_n(v)$ is (in some sense) an integrable function.

Figure 4 gives values of P_d as a function of the signal-to-noise power ratio S/N, for detection of a single pulse (no integration), and a linear-rectifier detector (sometimes

---

*In this section, reference to figures is to those of Part 1 (NRL Report 6930).

referred to as an envelope detector). The equations for $p_n(v)$ and $p_{sn}(v)$ for this case, as has been shown by North (2) and others, are

$$P_n(v) = \frac{v}{\sigma^2} e^{-v^2/2\sigma^2} \tag{12}$$

and

$$P_{sn}(v) = \frac{v}{\sigma^2} e^{-(v^2/2\sigma^2 + S)} I_0\left(\frac{v}{\sigma}\sqrt{2S}\right), \tag{13}$$

where σ^2 is the noise power at the detector input, and S is the signal-to-noise power ratio at the same point. These equations assume a Gaussian distribution for the amplitude of the RF noise voltage. This assumption is valid for the noise sources ordinarily present. (I_0 denotes the modified Bessel function of the order zero, which is related to the ordinary zero-order Bessel function J_0 by: $I_0(x) = J_0(ix)$; $i = \sqrt{-1}$. Equation (12) is the probability density function of a Rayleigh distribution, and that of Eq. (13) is sometimes referred to as the Rician distribution (after S.O. Rice (3), who described its properties in detail, although it had also been described previously by North and others.)

The function of Eq. (12) is integrable. Therefore, Eq. (11) can be solved for v_t. The result is

$$P_{fa} = e^{-v_t^2/2\sigma^2} . \tag{14}$$

Therefore,

$$\frac{v_t}{\sigma} = \sqrt{-2 \log_e P_{fa}} . \tag{15}$$

The ratio v_t/σ is the ratio of the threshold voltage to the predetection rms noise voltage. It is more practical to express v_t in relation to the average noise voltage at the detector *output* (since this quantity is easily measured; it is the dc output voltage of the detector). Since

$$\bar{v} = \int_0^\infty v p_n(v) \, dv = \sigma\sqrt{\pi/2} , \tag{16}$$

it follows that

$$u_t = \frac{v_t}{\bar{v}} = \sqrt{-4 \log_e P_{fa}/\pi} . \tag{17}$$

Robertson (4) has normalized the threshold voltage differently; the relationship of his threshold voltage, u_r, to the one used here, u_t, is

$$u_r = \frac{(u_t - 1)\sqrt{M}}{\sqrt{4/\pi - 1}} . \tag{18}$$

where M is the number of pulses integrated ($M = 1$ for Eq. (17)).

Results for u_t and also u_r, obtained by digital computer solution of Eqs. (17) and (18), are listed in Table 1. The values of u_r in Table 1 agree with those reported by Robertson (4), as do also the values of $P_d(S)$ plotted in Fig. 4. This agreement is noteworthy because the methods of computation were entirely different; Robertson employed a series representation of the solution for P_d, rather than direct numerical integration. His results are presented for a continuous range of values of P_{fa}, but the range is smaller than the one of Fig. 4. Robertson's curves are for discrete values of S in decibels ranging from +6 to +14.

Table 1
Values of Single-Pulse Normalized
Threshold Voltage for a Set of False-
Alarm Probabilities

P_{fa}	u_t	u_r
10^{-1}	1.7122	1.3625
10^{-2}	2.4215	2.7193
10^{-3}	2.9657	3.7605
10^{-4}	3.4245	4.6381
10^{-5}	3.8287	5.4114
10^{-6}	4.1941	6.1105
10^{-7}	4.5301	6.7534
10^{-8}	4.8429	7.3517
10^{-9}	5.1367	7.9137
10^{-10}	5.4146	8.4453
10^{-11}	5.6788	8.9509
10^{-12}	5.9313	9.4340
10^{-13}	6.1735	9.8973
10^{-14}	6.4066	10.3431
10^{-15}	6.6315	10.7733
10^{-16}	6.8489	11.1893

These values of u_t were used in computing the curves of Fig. 4, Part 1, by numerical integration of Eq. (13), with v replaced by $u = v/\bar{v}$; that is,

$$P_d(S) = \int_{u_t}^{\infty} \frac{\pi}{2} u \ e^{-[(\pi u^2/4)+S]} \ I_0\left(u\sqrt{\pi S}\right) \ du \ . \tag{19}$$

The numerical integration was carried out to seven-significant-figure accuracy, and the results were machine-plotted. The original plot, of which Fig. 4 is a photographic reduction, was 15 by 15 inches, and the plotter accuracy is specified by the manufacturer to be ±0.005 inch or better.

The probability scale of Fig. 4 resembles a Gaussian probability scale, but it is not; it is a 1/4-power-law scale which has similar properties but is more convenient for machine computation. This scale is defined by the relationships

$$x = x_m \left(\frac{P_d^{1/4} - P_{min}^{1/4}}{0.5^{1/4} - P_{min}^{1/4}} \right), \quad P_d \leq 0.5 \ , \tag{20a}$$

and

$$x = x_m \left[2 - \frac{(1 - P_d)^{1/4} - P_{min}^{1/4}}{0.5^{1/4} - P_{min}^{1/4}} \right] , \quad P_d \geq 0.5 , \tag{20b}$$

where x_m is the midpoint of the scale, x is the actual coordinate corresponding to a probability P_d, and P_{min} is the minimum value of P_d (corresponding to $x = 0$).

It is interesting to note that the P_d curves are asymptotic at their low ends to the vertical line $P_d = P_{fa}$. This results from the fact that by definition P_d cannot be smaller than P_{fa}; in other words,

$$\lim_{S \to 0} P_d(S) = P_{fa} . \tag{21}$$

(This result is indicated by the fact that Eq. (13) becomes identical to Eq. (12) when $S = 0$, because $I_0(0) = 1$.) Of course, the meaning of "probability of detection" is purely formal in this region; it is not a useful concept when $P_d = P_{fa}$, and applications of Fig. 4 (and similar curves for other situations) should be restricted to the condition $P_d \gg P_{fa}$. However, the fact that the curves of Fig. 4 do in fact become asymptotic to the $P_d = P_{fa}$ line is a check on the correctness of the computations.

Detection of Two Integrated Pulses

As has just been shown, the functions $p_n(v)$ and $p_{sn}(v)$ are exactly known for detection of a single pulse. As will later be shown, when a sufficient number of pulses are integrated, approximate formulas which are very accurate can be given for p_n and p_{sn}. For two or just a few pulses integrated, neither the exact functions nor good analytic approximations can be found. The series approximation method used by Robertson is probably the best method of solution. However, another method can be used for the two-pulse case, although it becomes too cumbersome for more than two pulses. This method was used to compute the two-pulse value used in Fig. 5, Part 1. It was used partly because it is a method that, by its nature, provides an interesting check on more analytical methods, and partly because the author wanted to see if it could be done. It is a Monte Carlo method, utilizing the random-number generator which is an on-line function of the NRL CDC-3800 computer.

The procedure used was as follows. First, the function p_{sn}, expressed in the form of the integrand of Eq. (19), was "digitized" by dividing the values of v into increments of 0.01, and for each increment the value of p_{sn} was expressed as an integer equal to the rounded-off value of $100 \, p_{sn} = N$. Then a 10,000-element one-dimensional array was set up in which the values of v were the elements; each value of v was entered into the array N times, where N is related to $p_{sn}(v)$ as stated above. Because of the normalization property of p_{sn}, i.e.,

$$\int_0^\infty p_{sn}(v) \, dv = 1 ,$$

the division of the range of v into increments of 0.01, and the multiplication of p_{sn} by 100, the resulting 10,000-element array contains all the significant part of the p_{sn} function.

An array of this type was set up, in the digital computer, for each value of S, in decibels, ranging from 3.5 dB to 15.5 dB, in 0.5 dB steps. These arrays were stored on magnetic tape.

To compute $P_d(S)$, using these arrays and the Monte Carlo method, the array for a specified value of S was buffered into the computer core memory, and the random number function was used to select an integer in the range 1 to 10,000; each such integer has equal probability of being selected.* This integer is then used as the array index to select a value of v, designated v_1. This represents the detected voltage for the first echo pulse of a two-pulse pair. The procedure is then repeated to obtain a second-pulse voltage, v_2. The sum of these voltages, $v_s = v_1 + v_2$, then represents the voltage output of a two-pulse postdetection integrator.

This value v_s was then compared with the threshold voltage, v_t, corresponding to a desired value of false-alarm probability, P_{fa}. If $v_s > v_t$, a detection was considered to have occurred; if $v_s \le v_t$, detection did not occur. This "experiment" was repeated many times, and a running account was kept of the ratio of successes to the total number of trials. This ratio, when taken for a sufficient number of trials, is a good experimental value for $P_d(S)$. The trials were continued until this experimental value stabilized, as determined by the following criterion. The "running average" ratio of successful detections to total trials was stored at the end of each sequence of 1000 trials. When this average for ten successive times (a total interval of 10,000 "observations" of "pulse-pairs") did not deviate from the first of these ten values by more than 0.00025, the run was terminated, and the value of P_d at the termination was recorded. Typical numbers of trials required for satisfaction of this criterion ranged from about 30,000 to 150,000 (a "trial" here means a single "pulse-pair" addition). The 0.00025 criterion seems to have been adequately small for the accuracy needed. It was noticed, however, that smaller numbers of trials were needed to satisfy the criterion at very high values of P_d than for values below 0.9. After the fact, it seems probable that the accuracy criterion should be made more stringent at very high (or very low) values of P_d, but the value used was apparently adequate for the range of P_d considered.

About 20 minutes of computer time (on the CDC-3800) were used. However, it was realized, again after the fact, that this time could have been cut considerably if a test for all five values of threshold voltage had been made for each added pair of randomly selected voltages from the probability-density arrays. (Instead, the complete experiment was reperformed for each value of threshold voltage, corresponding to a specified false-alarm probability.)

As the foregoing discussion indicates, the procedure requires determination of the threshold voltage, v_t, for a given false-alarm probability. This in turn requires, in principle, that the function p_n be given analytically. (It is not required that the function be analytically integrable, as it happens to be for the single-pulse case. If p_n is not analytically integrable, P_{fa} can be found by numerical integration, for a specified value of v_t. However, finding v_t for a specified P_{fa} then requires either interpolation or iteration.)

The function p_n for the two-pulse case cannot be obtained as an analytic function. Neither is it feasible to find P_{fa} by the same Monte Carlo method that has just been described for finding P_d. This method is feasible only for probabilities that are neither too small nor too large, because if the ratio of successes or failures to total trials in the Monte Carlo experiment is too small, an excessive number of trials is required for the value to stabilize — that is, to reduce the error to an acceptable value. It was successfully used for $P_d = 0.95$, but it would probably not be feasible, for example at

---

*The author is aware of limitations on the "randomness" of most so-called random-number generators, but analysis of the method and of the results indicates that these limitations did not affect the validity of the procedure described here.

$P_d = 0.999$, or 0.001. For P_{fa} values such as 10^{-6} or smaller, it would be out of the question.*

However, the following method proved to be practical. The probability density $p_{n(2)}$, for two pulses, is related formally to $p_{n(1)}$ by the following expression:

$$p_{n(2)}(z) = \int_0^z p_{n(1)}(x) \, p_{n(1)}(z-x) \, dx \ . \tag{22}$$

The proof of this formula follows directly from the assumption that the voltages of two successive samples of the detector output are statistically independent, and the two following propositions of probability theory: (1) the probability of the simultaneous occurrence of two independent events is the product of their separate probabilities, and (2) the probability of any single event is equal to the sum of the probabilities of the exhaustive and mutually exclusive possibilities of its occurrence. The product of the two terms of the integral represents the application of proposition (1), and the integral itself is an expression of proposition (2).

Since $p_{n(1)}$ is given by Eq. (12), the form of Eq. (22) in the present instance, taking $\sigma = 1$ for convenience, is

$$p_{n(2)}(z) = \int_0^z x \, e^{-x^2/2} \, (z-x) \, e^{-(z-x)^2/2} \, dx \ . \tag{23}$$

After some manipulation this can be expressed in the form†

$$p_{n(2)}(z) = e^{-z^2/4} \left[(z^2/2 - 1) \int_0^{z/2} e^{-u^2} \, du \right] + \frac{z}{2} \, e^{-z^2/2} \ . \tag{24}$$

The false-alarm probability is now related to this result by Eq. (11). After further manipulation, this yields:

$$P_{fa} = \int_{z_t}^{\infty} p_{n(2)}(z) \, dz$$

$$= 0.5 \, e^{-z_t^2/2} + \int_{z_t}^{\infty} \left[e^{-z^2/4} \, (z^2/2 - 1) \int_0^{z/2} e^{-u^2} \, du \right] dz \ . \tag{25}$$

---

*Dr. G. V. Trunk of the NRL Radar Division Analysis Staff, who reviewed portions of this report, has advised the author that he has used the Monte Carlo method to calculate probability of detection for N pulses, with N > 2 . He employed the characteristic function of the single-sample noise probability density to find the N-integrated-sample density function, and from this he determined the threshold voltage for specified false-alarm probability. He then employed the Monte Carlo method, as described here for two pulses, to compute probability of detection. (This method is basically applicable to any number of pulses, once the required threshold voltage has been determined.) Trunk has also found it feasible to use the Monte Carlo method for detection probabilities as low as 0.001.

†I am indebted to Dr. G. V. Trunk of the Radar Division Radar Analysis Staff for discovering an algebraic error in my initial derivation of this result, and for helpful discussions of other matters relating to the computation of detection probabilities.

The numerical solution of this formula requires a double numerical integration, but this is easily accomplished by the digital computer. The infinite upper limit of the integral is sufficiently well approximated by integrating to the numerical upper limit 25. (The result obtained for the overall integral of Eq. (25) by numerically integrating from 0 to 25 differs insignificantly from 0.5, which is the analytically correct result, since for $z_t = 0$ in Eq. (25), the result must be $P_{fa} = 1$.)

Since Eq. (25) was obtained by assuming $\sigma = 1$, the average voltage output for one noise sample is $\sqrt{2\pi}$, in accordance with the well-known theorem of probability theory for the average of the sum of two independent random variables. Therefore, the threshold voltage of Eq. (25) is related to threshold u_t (normalized to the average voltage) by the relation

$$u_t = z_t / \sqrt{2\pi} . \tag{26}$$

Since the expression derived finds P_{fa} when z_t is specified, and actually it is P_{fa} that is specified in probability of detection calculations, z_t was found for specified values of P_f by an interpolation procedure. The results for a range of values of P_{fa} are given in Table 2, in terms of the normalized quantity u_t. Also the equivalent threshold values u_r, normalized according to Robertson's method (4) (Eq. (18) with $M = 2$), are given.

Table 2
Values of Normalized Threshold Voltage
for Two-Pulse Detection

P_{fa}	u_t	u_r
10^{-4}	2.644	4.448
10^{-6}	3.168	5.866
10^{-8}	3.613	7.069
10^{-10}	4.006	8.133
10^{-12}	4.363	9.099

The resulting values of signal-to-noise ratio for specified probabilities of detection are given in Table 3. These results agree well (as closely as reading curves can affirm) with Robertson's results within the range of values of P_{fa} for which they overlap, and the values of u_r given in Table 2 also agree well with those published by Robertson. This is an excellent confirmation of both calculations, since the methods were radically different.

Table 3
Signal-to-Noise Ratios for Detection With Specified
Probability, Two Pulses Integrated

False-Alarm Probability	Signal-to-Noise Ratio (dB) for Various Probabilities of Detection					
	0.1	0.25	0.5	0.75	0.90	0.95
10^{-4}	3.85	5.48	6.95	8.22	9.20	9.74
10^{-6}	6.28	7.51	8.69	9.71	10.56	11.02
10^{-8}	7.87	8.87	9.88	10.78	11.52	11.94
10^{-10}	9.05	9.95	10.84	11.65	12.31	12.68
10^{-12}	9.97	10.79	11.59	12.33	12.96	13.31

In the Monte Carlo procedure for determining P_d, these values of u_t were rounded off to two decimal places, since that was the limit of accuracy set by the number of elements in the digitized arrays of detector output voltages.

Detection with Many Pulses Integrated

Although the method that has been described for detection of two pulses cannot practically be applied for even three pulses, and certainly not for many pulses, certain approximations can be made for the functions p_n and p_{sn} of Eqs. (10) and (11) in the many-pulse case which become very good if the number of pulses is sufficiently large. These approximations are described by North (2). They make use of the central limit theorem of probability theory, which states that the distribution of the sum of n independent random variables tends to a Gaussian (or normal) form as n tends to infinity, no matter what the distributions are for the individual variables, subject to some fairly mild conditions that are well satisfied in the present situation. The variances and average values of these sum distributions are found by applying the following two well-known theorems: (1) the standard deviation σ_M for the sum of M independent random variables is given by

$$\sigma_M^2 = \sum_{i=1}^{M} \sigma_i^2 , \tag{27}$$

where σ_i is the standard deviation of the ith variable; (2) the average of the sum, $\bar{x}_M$, is given by

$$\bar{x}_M = \sum_{i=1}^{M} \bar{x}_i , \tag{28}$$

where x_i is the average value of the ith variable.

The desired Gaussian density functions for the detector output voltage v are therefore

$$p(v) = \frac{1}{\sqrt{2\pi}\ \sigma_o} e^{-(v-\bar{v})^2/2\sigma_o^2} , \tag{29}$$

where σ_o and $\bar{v}$ are found by applying Eqs. (27) and (28). Since a steady signal and constant noise power are assumed, all the $\bar{v}_i$'s and σ_i's in these equations are equal; hence for M pulses integrated the results are

$$\bar{v}_M = M\ \bar{v}_1 \tag{30}$$

and

$$\sigma_M = \sqrt{M}\ \sigma_1 . \tag{31}$$

The quantity σ_o in Eq. (29) is the standard deviation of the detector *output* voltage, which is not the same as that of the input voltage, denoted σ in Eqs. (12) and (13). The relationships of $\bar{v}_1$ and σ_1 to the detector-input quantity σ for the noise-only case are

$$\bar{v}_{1n} = \sigma \sqrt{\pi/2} \tag{32}$$

and

$$\sigma_{1n} = \sigma \sqrt{2 - \pi/2} = \bar{v}_{1n} \sqrt{(4/\pi) - 1} \ . \tag{33}$$

For the signal-and-noise case the relationships are*

$$\bar{v}_{1sn} = \sigma \sqrt{\frac{\pi}{2}} \cdot b = b\bar{v}_{1n} \ , \tag{34}$$

$$\sigma_{1sn} = \bar{v}_{1n} \sqrt{(4/\pi)(1+S) - b^2} \ , \tag{35}$$

and

$$b = e^{-S/2} [(1+S) I_0(S/2) + S \cdot I_1(S/2)] \ . \tag{36}$$

(For $S = 0$, $b = 1$, since $I_0(0) = 1$ and $I_1(0) = 0$.)

The false-alarm probability is then given by

$$P_{fa} = \frac{1}{\sqrt{2\pi}\ \sigma_{Mn}} \int_{v_t}^{\infty} e^{-(v-\bar{v}_{Mn})^2/2\sigma_{Mn}^2} \ dv \ , \tag{37}$$

and the probability of detection is

$$P_d = \frac{1}{\sqrt{2\pi}\ \sigma_{Msn}} \int_{v_t}^{\infty} e^{-(v-\bar{v}_{Msn})^2/2\sigma_{Msn}^2} \ dv \ , \tag{38}$$

where v_t is the selected threshold voltage.

Integrals of the type shown can be written in terms of the error function,

$$\mathrm{erf}(u) = \frac{2}{\sqrt{\pi}} \int_0^u e^{-t^2} \ dt \ , \tag{39}$$

which is a tabulated function. For computer programs, standard subroutines for $\mathrm{erf}(u)$ are available; alternatively, direct numerical integration can be employed.

In terms of this function, and with quantities in the arguments of the error function normalized to the average noise output (for M added samples), and with the normalized threshold voltage written as $u(t)$, the equations for false-alarm probability and probability of detection become

$$P_{fa} = \frac{1}{2} - \frac{1}{2} \ \mathrm{erf} \left[\frac{u_t - 1}{\sqrt{2(4/\pi - 1)/M}} \right] . \tag{40}$$

---

*See S. O. Rice, Ref. 3, Eqs. 4.2-3 and 4.2-6, pages 119-120. The notation $I_n(x)$ in Eq. (36) stands for the modified Bessel function of the first kind, of order n. For nonnegative integral values of n, it is related to the ordinary Bessel function $J_n(x)$ by the formula $I_n(x) = i^{-n} J_n(ix)$; $i = \sqrt{-1}$.

This equation can be solved for u_t by iteration, or by interpolation using a table of the error function. For some standard values of P_{fa} the iteration can be done "in general" to find a constant k_{pfa}, such that

$$u_t = 1 + k_{pfa} \sqrt{2(4/\pi - 1)/M} . \tag{41}$$

The formula for k_{pfa} is

$$k_{pfa} = erf^{-1}(1 - 2 P_{fa}) , \tag{42}$$

where the notation erf^{-1} denotes the "inverse error function." Some useful values of k_{pfa}, which were obtained by interpolation using a 15-place table of the error function,* are given in Table 4.

Table 4
Values of Inverse Error Function, k_{pfa}, for Some Standard Value of False Alarm Probability,

P_{fa}	k_{pfa}
10^{-4}	2.630
10^{-6}	3.361
10^{-8}	3.968
10^{-10}	4.498
10^{-12}	4.974

The corresponding equation for P_d is

$$P_d = \frac{1}{2} - \frac{1}{2} erf \left[\frac{u_t - b}{\sqrt{2[4(1+S)/\pi - b^2]/M}} \right]. \tag{43}$$

Again, a constant can be found for a specified value of P_d:

$$k_{pd} = erf^{-1}(1 - 2 P_d) . \tag{44}$$

In terms of this constant Eq. (43) becomes

$$\frac{u_t - b}{\sqrt{2[4(1+S)/\pi - b^2]/M}} = k_{pd} . \tag{45}$$

However, this equation cannot be solved explicitly for S, because b is a function of S. If the explicit expression for b is used (Eq. (36)), it becomes evident that an algebraic solution is not possible. Consequently, iteration is required for numerical solution of Eq. (45) for S, just as it would be if Eq. (43) were used directly. Nevertheless, the procedure of finding k_{pd} and writing Eq. (45) is advantageous when solutions for several or

*For small values of P_{fa}, a many-place table is required, such as the 15-place "Tables of Probability Functions," Vol. 1, WPA Tables, U.S. Govt. Printing Office, 1941. These tables are adequate for $P_{fa} \geqq 10^{-12}$.

many values of N are desired for the same value of P_d, because the iterative solution of Eq. (45) does not involve numerical integration, as does that of Eq. (43). Values of k_{pd} for some standard values of P_d are given in Table 5. These were obtained by iteration using the CDC-3800 computer and an error-function subroutine. It is noteworthy that

$$k_{pd}(P_d) = -k_{pd}(1-P_d) \; , \tag{46}$$

so that one iteration procedure gives values of k_{pd} for two values of P_d. Also, for $P_d = 0.5$, $k_{pd} = 0$ exactly.

Table 5

Values of Inverse Error Function, k_{pd}, for Some Standard Values of Probability of Detection, P_d

P_d	k_{pd}
0.01	1.644976
0.05	1.163087
0.10	0.9061940
0.25	0.4769363
0.50	0.0000000
0.75	-0.4769363
0.90	-0.9061940
0.95	-1.163087
0.99	-1.644976

This "many-pulse" method for computing P_d is, of course, useful only if some idea can be given of the errors incurred in using it for various numbers of pulses. Table 6 compares the results obtained using this method and the results published by Robertson (4), for some representative cases. Robertson's results were calculated for numbers of pulses that are integral powers of two — i.e., for $M = 1, 2, 4, 8, \ldots$, to a maximum of $8192 \; (= 2^{13})$. Table 6 makes the comparison for several of these values of M, for two values of probability of detection, and for those values of false-alarm probability for which the two sets of results overlap. It was difficult to read Robertson's curves to better than about 0.1 dB; the figures given, therefore, sometimes read to the nearest 0.1 dB, sometimes to one more decimal place. The decibel discrepancy was, however, in all cases rounded off to the nearest 0.1 dB. It is evident that the agreement improves, as would be expected, as the number of pulses increases — because the assumption of Gaussian density curves for p_n and p_{sn} (Eqs. (10) and (11)) is more nearly correct as the number of pulses integrated increases (in accordance with the central limit theorem). It is probably a good rule of thumb that the method is virtually exact for numbers of pulses in the thousands, very good for numbers in the hundreds (error of order 0.1 dB), and in error by roughly 0.5 dB at about ten pulses integrated.

It will be evident to the reader that Robertson's results have been used as a check on the correctness of results obtained for each of the three computational procedures employed (for one, two, and many pulses integrated). It might thus seem that it would have been simpler in the first place to plot the curves desired using Robertson's results, or to use his method for computing the plotted points. As a matter of fact, the procedures described here were developed before Robertson's paper was published. Moreover, his paper does not give the details of his computational procedure. Quite apart from these practical factors, however, there are several justifications for carrying out the procedure that has been described. First, just as Robertson's results confirm the correctness of the results obtained here, so also do these results confirm Robertson's. Second, the

Table 6
Comparison of North and Robertson Methods for
Several Values of Parameters

No. of Pulses	False-Alarm Probability	Probability of Detection	Signal-to-Noise Ratio (dB)		Discrepancy (dB)
			North's Method	Robertson's Curves	
8	10^{-4}	0.5	2.14	2.70	0.6
		0.9	4.26	4.60	0.3
	10^{-6}	0.5	3.42	4.1	0.7
		0.9	5.23	5.8	0.6
32	10^{-4}	0.5	-1.25	-0.95	0.3
		0.9	0.54	0.70	0.2
	10^{-6}	0.5	-0.08	0.28	0.4
		0.9	1.44	1.72	0.3
128	10^{-4}	0.5	-4.45	-4.3	0.2
		0.9	-2.88	-2.8	0.1
	10^{-6}	0.5	-3.33	-3.19	0.1
		0.9	-2.02	-1.90	0.1
4096	10^{-4}	0.5	-12.13	-12.1	0
		0.9	-10.80	-10.8	0
	10^{-6}	0.5	-11.06	-11.02	0
		0.9	-9.96	-9.95	0
	10^{-8}	0.5	-10.33	-10.1	0.2
		0.9	-9.38	-9.45	0.1

curves that have been plotted here cover a range of values of the false-alarm probability not available in Robertson's published paper. Finally, the methods employed here are inherently interesting, for various reasons; they illuminate some of the theory of detection — especially the Monte Carlo procedure for the two-pulse case, since it is based partly on a mathematical analysis and partly on a statistical experiment. It is intermediate between a purely mathematical solution and an experimental one in which an actual threshold device with real signals and noise would be employed.

Curve Plotting Procedure

The curves of Figs. 5 through 22, Part 1, were plotted by machine. The plotter used for these curves was the Gerber Model 875, which plots to an accuracy of ±0.005 inch or better, with overall plot dimensions up to 5 by 8 feet. The plots were made to a size of 16 by 20 inches, and photographically reduced for use in this report. The coordinate grid was also done by the machine, to avoid any problems of registration which would arise if the plotting were done on ready-made coordinate paper. (The coordinate-axis numbering and labeling was also done by the machine.)

Since points of the curves were computed for a limited set of values of the number of pulses, a plotting subroutine was used which computes interpolated points to produce a smooth curve, in much the same manner that a draftsman would use a French curve. (The subroutine, written by the author, is named FCURVE.)

To avoid possible inaccuracy, the "many-pulse" method was used for Figs. 5 through 10 only for very large numbers of pulses. After some experimenting it was found that curves of best accuracy (as judged by comparison with Robertson's curves) could be produced by computing five points, at M = 1, 2, 8000, 9000, and 10,000 pulses. The latter three points establish a slope at the many-pulse end of the curve, and the one- and two-pulse points establish a slope at the low end. The FCURVE subroutine provides the required transition between these slopes. This method produced a better agreement with Robertson's results, in the region of overlap, than did computation of additional points with the many-pulse method. The agreement finally produced is as good, for all numbers of pulses, as the readability of the curves.

In accordance with theory, the slope of these curves is asymptotic to -1.5 dB per octave in the small-signal region (S/N << 1), and to -3 dB per octave in the large-signal region (S/N >> 1). That is, S/N $\propto M^{-1}$ for S/N >> 1 and S/N $\propto M^{-1/2}$ for S/N << 1. Robertson has noted that his results are similarly in agreement with these asumptotic values.

Results for Fluctuating Signals

Figures 6 and 7 of Part 1, which are for the Swerling Cases 1 and 3 types of fluctuating signals, were plotted in the manner just described, with points computed using a computer program due to Fehlner et al. of the Johns Hopkins University Applied Physics Laboratory, and described in Ref. 5. It is essentially a confirmation, with some corrections, of the results of Marcum (6) and Swerling (7). It was modified by the author and by Stanley Gontarek* to permit it to run on the CDC-3800 computer instead of on an IBM machine for which it was written. It was further modified by the author to compute results with false-alarm probability as an input parameter, rather than Marcum's false-alarm number. Figures 6 and 7 are also plotted in the same format as Fig. 5, with number of pulses integrated and signal-to-noise ratio as coordinates and false-alarm probability as a family parameter. (The curves published by Robertson have, as coordinates, probability of detection and false-alarm probability; the family parameter is signal-to-noise ratio. Fehlner's curves have signal-to-noise ratio and probability of detection as coordinate axes, with Marcum's false-alarm number as the family parameter.)

In the literature of radar range calculation, there is sometimes defined a "fluctuating-signal loss," which is applied when the nonfluctuating-signal visibility factor has been used in a range calculation and it is desired to convert the result to apply to the fluctuating-signal case. As a casual inspection of Figs. 5 through 7 indicates, this concept is not tenable. The "loss" is sometimes a gain, and it cannot be related to any one of the other parameters. The relationship of the signal-to-noise ratio required for detection in the steady-signal case to that for fluctuating-signals does not permit a simple correction to be made. The correct procedure is to calculate the range using a visibility factor obtained from the appropriate curve of Figs. 5 through 7, or some similar curve appropriate to the applicable fluctuation model.

Calculation of Radar Range for Specified Target-Cross-
    Section Measurement Accuracy

In Part 1, radar "maximum range" equations are given for specified values of probability of detection and specified false-alarm probability. The foregoing sections of Part 2 have detailed the theory of this maximum-range concept, which is the appropriate

*Naval Air Systems Command.

one for most radar applications. However, in certain uses of radar, it is desired to know the range at which the signal-to-noise ratio will reach a specified value, rather than the range for a specified probability of detection. These are primarily measurement uses — that is, application in which the radar is being used to measure some characteristic of the radar target, such as its radar cross section. In these applications, the appropriate equation is Eq. (6) of Part 1, with the "max" and "min" subscripts removed.

The question to be answered in these applications is: how does the accuracy of the measurement depend on the signal-to-noise ratio?

Two cases (at least) can be considered. The first is that in which the desired measurement is to be made on the basis of a single received pulse (or a single sample of a CW signal, the sample time being equal to or less than the reciprocal of the receiver noise bandwidth). In the second case, the measurement is made after averaging a number of pulses or samples of the signal and noise. For the first case, assuming also that only reasonably small errors are to be permitted (so that only large signal-to-noise ratios are considered), the following analysis applies.*

If the receiving system were completely noise free, the measured receiver output signal would be an accurate measure of the signal power at the receiver input. The presence of noise, however, causes the receiver output voltage at a specific instant to be randomly somewhat greater or less than the value which would be observed under noise-free conditions. Accordingly, a measurement of this voltage made at any particular instant (i.e., for any single received pulse) will be in error by some amount that cannot be predicted. However, the statistics of this error can be calculated, as a function of the input signal-to-noise power ratio. The basic theory from which such calculation may be made has been developed by Rice (3) and others. A linear-rectifier detector is assumed. Also assumed is a linear receiver-amplification characteristic. Although in practice there may be some nonlinearity, correction for this nonlinearity can be made in processing the data.

The following notation will be used:

   P = amplitude of sine-wave RF input signal voltage,

   R = rms value of input RF noise voltage,

   S = $P^2/2R^2$, input signal-to-noise power ratio,

   v = receiver output voltage (video pulse voltage).

Rice has shown (Ref. 3, Eq. (4.2-5), p. 120) that, assuming a linear-rectifier detector, for large signal-to-noise ratios the average output voltage is asymptotically given by

$$\bar{v} \approx C\ (P + R^2/2P + R^4/8P^3 + \ldots)$$ (47)

and that the mean-square value (Rice, Eq. (4.2-6)) is

$$\overline{v^2} = C^2\ (P^2 + 2R^2) \ .$$ (48)

---

*This analysis is basically taken from the author's Appendix A of Ref. 8, but has been extended to apply to target-cross-section measurement.

(In these expressions C is a constant proportional to the voltage gain of the receiver.) Therefore the variance σ^2 of v is (neglecting terms of order higher than $R^2/2P^2$)

$$\sigma^2 = \overline{v^2} - \overline{v}^2 = C^2R^2(1 - R^2/2P^2) , \tag{49}$$

corresponding to Rice's Eq. (4.2-7). Hence the standard deviation is

$$\sigma = CR(1 - R^2/2P^2)^{1/2} . \tag{50}$$

Moreover, Rice has shown that for sufficiently large signal-to-noise ratios, the distribution of v is approximately normal, meaning that the probability density is given very nearly by

$$p(v) = \frac{1}{\sqrt{2\pi}\,\sigma} \exp[-(v - \overline{v})^2/2\sigma^2] . \tag{51}$$

The probability that the observed voltage deviates from the average value, $\overline{v}$, by more than a specified amount Δv is therefore given by

$$\mathscr{P} = \text{Prob.}\left(|v - \overline{v}| > \Delta v\right) = 2 \int_{\overline{v}+\Delta v}^{\infty} P(v)\, dv . \tag{52}$$

For a given deviation, say $\Delta v = k\sigma$, the fractional error of the voltage measurement, $\Delta v/\overline{v}$, from Eqs. (47) and (50), is (again neglecting higher-order terms) approximately

$$\frac{\Delta v}{\overline{v}} = \frac{k\sigma}{\overline{v}} \approx \frac{kR(1 - R^2/2P^2)^{1/2}}{(P + R^2/2P + R^4/8P^3)}$$

$$\approx \frac{kR}{P}\left[\frac{(1 - R^2/2P^2)^{1/2}}{(1 + R^2/2P^2 + R^4/8P^4)}\right]$$

$$\approx \frac{k}{\sqrt{2S}}\left[\frac{(1 - 1/4S)^{1/2}}{(1 + 1/4S + 1/32S^2)}\right] , \tag{53}$$

in which S, as previously noted, is the input signal-to-noise power ratio. Inasmuch as it has already been assumed, in deriving this expression, that S is much larger than unity, the term in brackets will ordinarily be approximately equal to unity, so that for most calculations the simple formula

$$\frac{\Delta v}{\overline{v}} \approx \frac{k}{\sqrt{2S}} \tag{54}$$

may be used.

This analysis relates the accuracy of the signal voltage measurement (after detection) to the predetection signal-to-noise ratio. In many applications, although this voltage ($\overline{v}$) is the directly measured quantity, the ultimate objective is measurement of the

radar cross section* of the target, σ_t. This is accomplished through the following relation (which applies, as may be deduced from Eq. (47), when the detector is linear and the signal-to-noise ratio is large, because P is proportional to σ_t):

$$\sigma_t = k_c \bar{v}^2 R^4/F^4 , \tag{55}$$

where k_c is a calibration constant, usually evaluated by observing a "standard target" whose radar cross section is known — for example, a conducting sphere; R is the radar range; and F is the pattern-propagation factor.

From Eq. (55) a relationship between the fractional error of measurement of $\bar{v}$ and the corresponding error of measurement of σ_t can be written. The procedure is first to write the difference equation:

$$\sigma_t + \Delta\sigma_t = k_c (\bar{v} + \Delta v)^2 R^4/F^4 , \tag{56}$$

where $\Delta\sigma_t$ is an increment of σ_t corresponding to the voltage increment Δv. This leads to the result

$$\frac{\Delta\sigma_t}{\sigma_t} = 2 \left(\frac{\Delta v}{\bar{v}}\right) + \left(\frac{\Delta v}{\bar{v}}\right)^2 . \tag{57}$$

Equation (52) can be rewritten as follows in terms of a new variable $t = (v - \bar{v})/\sigma$:

$$\mathscr{P} = \frac{2}{\sqrt{2\pi}} \int_{\Delta v/\sigma}^{\infty} e^{-t^2/2} \, dt = 1 - \frac{2}{\sqrt{2\pi}} \int_{0}^{\Delta v/\sigma} e^{-t^2/2} \, dt . \tag{58}$$

The quantity

$$E(k) = \frac{2}{\sqrt{2\pi}} \int_{0}^{k} e^{-t^2/2} \, dt , \tag{59}$$

sometimes known as the error integral, is a tabulated function, and is also readily evaluated by numerical integration using a computer. The latter method was used here. For various values of k and S, $\mathscr{P}$ was found from Eq. (58), $\Delta v/\bar{v}$ was found from Eq. (54), and $\Delta\sigma_t/\sigma_t$ was found from Eq. (57). Figure 1 is a plot of $\mathscr{P}$ as a function of $\Delta\sigma_t/\sigma_t$ with S (in decibels) as a parameter.

For Case 2, in which many pulses are averaged, the signal-to-noise ratio is generally small, typically much less than 1. Again assuming a linear detector, the average detector output when there is no signal is given by Eq. (32), and with a signal present it is given by Eq. (34). These two averages are related by the factor b, Eq. (36). The question is then, what is the limitation on the accuracy imposed by the fluctuations in the measured values of the quantities $\bar{v}_{sn}$ and $\bar{v}_n$?

---

*It is unfortunate in the following discussion that the symbol σ is used for both target cross section and for the standard deviation of signal and noise voltages. This is done because σ is the standard symbol for both of these quantities. The subscript t will be used whenever a target cross section is meant.

Fig. 1 – Probability of specified errors in single-pulse measurement of radar cross section
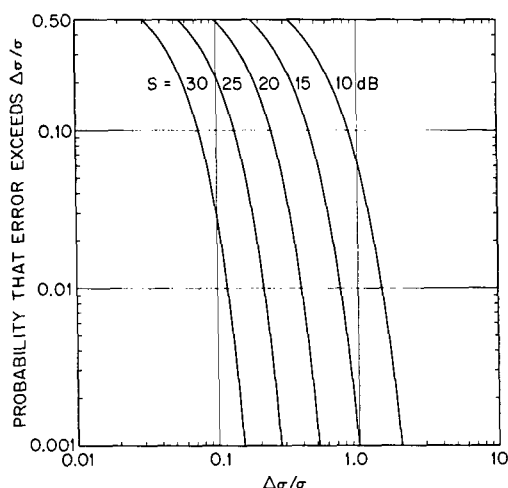
The analysis that follows is based on the assumption that the signal-to-noise power ratio, S, is very small (much less than 1), the opposite of the assumption made for the one-pulse measurement case. (The intermediate situation is much more difficult to analyze, but the results of an analysis would necessarily be intermediate between those of the two limiting cases.) Postdetection integration of M pulses is assumed.

The small-argument approximation for the exponential and modified Bessel functions, appropriate when $S \ll 1$, result in the following first-order approximation of Eq. (36):

$$b = 1 + S/2 .$$ (60)

Applying this result to Eq. (34) and solving for S gives

$$S = 2 \left[\frac{\bar{v}_{1sn} - \bar{v}_{1n}}{\bar{v}_{1n}} \right] .$$ (61)

For a single pulse, Eqs. (33) and (35) relate σ_{1n} and σ_{1sn} to $\bar{v}_{1n}$. Applying Eq (60) to Eq. (35) shows that for $S \ll 1$, $\sigma_{1n} \approx \sigma_{1sn}$, so that only Eq. (33) is needed:

$$\sigma_{1sn} \approx \sigma_{1n} = \bar{v}_{1n} \sqrt{4/\pi - 1} .$$ (62)

If M pulses are integrated,

$$\sigma_{Mn} = \sqrt{M}\, \sigma_{1n}$$ (63)

and

$$\bar{v}_M = M v_1 .$$ (64)

(See Eqs. (30) and (31).) Therefore

$$\sigma_{Mn} = \frac{\bar{v}_{Mn}}{\sqrt{M}} \sqrt{4/\pi - 1}$$ (65)

and

$$S = 2 \left[\frac{\bar{v}_{Msn} - \bar{v}_{Mn}}{\bar{v}_{Mn}} \right] = \frac{2D_M}{\bar{v}_{Mn}} . \tag{66}$$

Again a difference equation can be written:

$$S + \Delta S = \frac{2(D_M + \Delta D_M)}{\bar{v}_{Mn}} . \tag{67}$$

Here $\bar{v}_{Mn}$ is treated as a constant, since it can be measured with much greater accuracy, ordinarily, than can $\bar{v}_M$, or D_M, because it can be averaged over a much longer time period.

Dividing by S on the left and by $2D_M/\bar{v}_{Mn}$ on the right gives

$$\frac{\Delta S}{S} = \frac{\Delta D_M}{D_M} . \tag{68}$$

Since S is directly proportional to the target cross section σ_t, this means that the percentage error in measurement of σ_t is equal to the corresponding error in measurement of D_M. When the number of pulses integrated is large, the probability density function of D_M is normal (gaussian). (This is approximately true for as few as ten pulses integrated.) Therefore the procedure followed in the one-pulse error analysis (Eq. (52)) can be applied. The equation corresponding to Eq. (53) (making use of Eqs. (65) and (66), and recalling that the standard deviation of D_M is σ_{Mn}) is

$$\frac{\Delta \sigma_t}{\sigma_t} = \frac{\Delta D_M}{D_M} = \frac{k\sigma_{Mn}}{D_M} = \frac{2k}{S\sqrt{M}} \sqrt{4/\pi - 1} . \tag{69}$$

Combining all of the numerical factors and omitting the intermediate expressions gives

$$\frac{\Delta \sigma_t}{\sigma_t} = 1.0454 \frac{k}{S\sqrt{M}} . \tag{70}$$

Following the same procedure described for Fig. 1 results in a similar plot, Fig. 2, with $S\sqrt{M}$ as the parameter instead of S.

The foregoing analysis applies to the pulse-radar measurement of a point-target radar cross section. Another situation will now be treated briefly because it applies to a practical problem of some importance — the measurement of the signal power returned from a volume distribution of independently random scattering elements. This situation arises for example in measurement of the Thomson scatter echo from the ionosphere, which is used to determine the electron-density profile. Other examples are echoes from rain and from "chaff" (a cloud of metallic reflectors used as a radar countermeasure). The problem will be discussed in terms of the Thomson scatter echo, but the results are applicable to the other examples also. This echo signal is well known to be a Gaussian-noise-like signal, so that its effect is to increase the level of the receiver noise already present. The statistics of the combined signal and noise are therefore identical to those of the receiver noise, and Eqs. (29), (32), and (33) apply. Moreover, if the Thomson scatter signal power at the input of a linear detector is w_{TS}, the standard deviation is $\sigma_{TS} = \sqrt{w_{TS}}$, and the standard deviation of the total power at the same point is

Fig. 2 – Probability of specified errors in many-pulse measurement of radar cross section
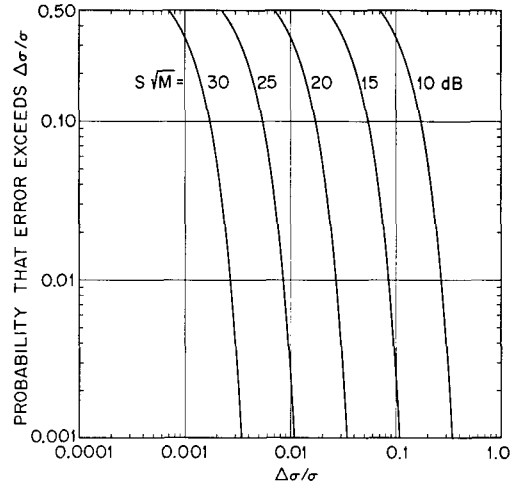
$$\sigma_{sn} = \sqrt{\sigma_{TS}^2 + \sigma_n^2} \;, \tag{71}$$

where σ_n is the standard deviation of the receiver noise. Therefore,

$$w_{TS} = \sigma_{sn}^2 - \sigma_n^2 \;. \tag{72}$$

From Eq. (32), the average detector output voltages $\bar{v}_{sn}$ and $\bar{v}_n$ can be substituted on the right-hand side, giving

$$w_{TS} = \frac{2}{\pi} \left(\bar{v}_{sn}^2 - \bar{v}_n^2 \right) \;. \tag{73}$$

Thus the desired measurement of w_{TS} can be made by measuring the observable quantities $\bar{v}_{sn}$ and $\bar{v}_n$, the average detector output voltages when the Thomson scatter signal is present and absent.

Again it will be assumed that $\bar{v}_n$ can be measured much more accurately than $\bar{v}_{sn}$, so that the error in determining w_{TS} is due primarily to the error of measurement of $\bar{v}_{sn}$. The relationship of the fractional error in measurement of w_{TS} to that of $\bar{v}_{sn}$ can as before be obtained by writing a difference equation, which after some manipulation yields

$$\frac{\Delta w_{TS}}{w_{TS}} = \frac{2\bar{v}_{sn}\,\Delta v_{sn} + \Delta v_{sn}^2}{\bar{v}_{sn}^2 - \bar{v}_n^2} \;. \tag{74}$$

Making use of Eqs. (32) and (71), the denominator on the right can be rewritten in the form

$$\bar{v}_{sn}^2 - \bar{v}_n^2 = \bar{v}_{sn}^2 \left(\frac{S}{S+1} \right), \tag{75}$$

in which $S = \sigma_{TS}^2 / \sigma_n^2$ is the input signal-to-noise power ratio. Eq. (74) thus becomes

$$\frac{\Delta w_{TS}}{w_{TS}} = \left(\frac{S + 1}{S}\right) \left[2 \left(\frac{\Delta v_{sn}}{\overline{v}_{sn}}\right) + \left(\frac{\Delta v_{sn}}{\overline{v}_{sn}}\right)^2\right] . \tag{76}$$

This equation applies for "single sample" measurement of $\overline{v}_{sn}$. In this case the probability density function is not gaussian (Eq. (29)); it is the Rayleigh function (Eq. (12)). The Rayleigh probability density function for a single sample of the signal-plus-noise output is

$$p(v) = \frac{\pi v}{2\overline{v}^2} e^{-\pi v^2/4\overline{v}^2} . \tag{77}$$

(This equation is equivalent to Eq. (12) except that it is in terms of $\overline{v}$ rather than σ, since $\overline{v}_{sn}$ is the quantity to be measured; see also Eq. (32).) The probability of making a measurement error exceeding Δv is therefore

$$\mathcal{P} = 1 - \int_{\overline{v}-\Delta v}^{\overline{v}+\Delta v} \frac{\pi v}{2\overline{v}^2} e^{-\pi v^2/4\overline{v}^2} dv . \tag{78}$$

This integration is performed by making the change of variable $u = \pi v^2/4\overline{v}^2$, whereupon

$$\mathcal{P} = 1 - \int_{L_1}^{L_2} e^{-u} du = 1 - e^{-L_2} + e^{-L_1} , \tag{79}$$

where

$$L_1 = \frac{\pi}{4\overline{v}^2} (\overline{v} - \Delta v)^2 = \frac{\pi}{4} \left[1 - 2\left(\frac{\Delta v}{\overline{v}}\right) + \left(\frac{\Delta v}{\overline{v}}\right)^2\right] \tag{80}$$

and

$$L_2 = \frac{\pi}{4\overline{v}^2} (\overline{v} + \Delta v) = \frac{\pi}{4} \left[1 + 2\left(\frac{\Delta v}{\overline{v}}\right) + \left(\frac{\Delta v}{\overline{v}}\right)^2\right] , \tag{81}$$

subject to the constraint $\Delta v \leqq \overline{v}$ (since the lower limit in Eq. (78) cannot be less than zero). When numerical results using this formula are examined, it is found that values of $\Delta v/\overline{v}$ corresponding to $\Delta w_{TS}/w_{TS}$ of the order of unity give values of $\mathcal{P}$ greater than 0.5, regardless of how large S becomes (since the factor $(S + 1)/S$ approaches unity asymptotically as S tends to infinity). This means that a one-pulse Thomson scatter measurement is subject to an unacceptably large probable error, as is well known by practitioners of this method of ionospheric measurement.

The measurement is customarily made, in Thomson scatter work, by averaging many samples which are statistically independent (corresponding to the signal returns from many successive pulses transmitted by the radar). The distribution of this average is asymptotically Gaussian, by the central limit theorem (discussed preceding Eq. (27)). Therefore $\mathcal{P}$ is calculated from the formula (similar to Eq. (58))

$$\mathcal{P} = 1 - \frac{2}{\sqrt{2\pi}} \int_0^k e^{-t^2/2} dt , \tag{82}$$

where k is $\Delta v / \sigma$. The relationship between k and $\Delta v / \bar{v}_{sn}$ is (applying Eq. (32))

$$\frac{\Delta v}{\bar{v}_{sn}} = \frac{k\sigma}{\bar{v}_{sn}} = \frac{k}{\sqrt{\pi/2}} \cdot \tag{83}$$

If M statistically independent samples are averaged, the standard deviation of the distribution of $\bar{v}_{sn}$ is reduced by the factor $\sqrt{M}$ compared to that of a single sample, as indicated by Eq. (31). Consequently, the probability decreases for exceeding a given value of $\Delta v / \bar{v}$ as M increases. That is, since the standard deviation of $\bar{v}_{sn}$ is reduced by the factor $\sqrt{M}$, so also is the value of Δv_{sn} corresponding to a probability $\mathcal{P}$ reduced by the same factor.

Consequently Eq. (76) can be rewritten in the form

$$\left(\frac{\Delta w_{TS}}{w_{TS}}\right)' = \left(\frac{S+1}{S}\right)\left[\frac{2}{\sqrt{M}}\left(\frac{\Delta v_{sn}}{\bar{v}_{sn}}\right) + \frac{1}{M}\left(\frac{\Delta v_{sn}}{\bar{v}_{sn}}\right)^2\right], \tag{84}$$

where $\left(\Delta w_{TS}/w_{TS}\right)'$ denotes the fractional error in measuring w_{TS} when M samples are averaged and $\Delta v_{sn}/\bar{v}_{sn}$ is the one-sample value. If

$$\frac{1}{2\sqrt{M}}\left(\frac{\Delta v_{sn}}{\bar{v}_{sn}}\right) \ll 1 \, , \tag{85}$$

the second term in the brackets of Eq. (84) can be neglected, and the equation can then be rewritten in the form

$$\sqrt{M}\left(\frac{S}{S+1}\right)\left(\frac{\Delta w_{TS}}{w_{TS}}\right)' = 2\,\frac{\Delta v_{sn}}{\bar{v}_{sn}} \cdot \tag{86}$$

Therefore if $\mathcal{P}$ is calculated for the one-sample value of $\Delta v_{sn}/\bar{v}_{sn}$, from Eq. (82), and the results plotted as a function of $2\,(\Delta v_{sn}/\bar{v}_{sn})$, the curve can be interpreted as applicable to the parameter $\sqrt{M}\,[S/(S+1)]\,(\Delta w_{TS}/w_{TS})$, as shown in Fig. 3, provided that M is actually appreciably greater than 1 (because Eq. (82) does not really apply for $M = 1$). (The prime symbol on $(\Delta w_{TS}/w_{TS})$ has been dropped, but is implied, in the labeling of the abscissa scale.)

After $(\Delta w_{TS}/w_{TS})$ has been found using this curve, for specified values of S, M, and $\mathcal{P}$, a test should be made to insure that Eq. (85) is satisfied. The equivalent relation in terms of $(\Delta w_{TS}/w_{TS})$ is

$$\left(\frac{\Delta w_{TS}}{w_{TS}}\right) \ll 4\left(\frac{S+1}{S}\right) \cdot \tag{87}$$

(This relation can always be satisfied by taking M sufficiently large.)

For some specified value of $\mathcal{P}$, a simple equation can be written for $(\Delta w_{TS}/w_{TS})$. For example, if $\mathcal{P} = 0.001$, the abscissa of the curve is 5.25. Therefore, for $\mathcal{P} = 0.001$,

$$\frac{\Delta w_{TS}}{w_{TS}} = \frac{5.25}{\sqrt{M}}\left(\frac{S+1}{S}\right) \cdot \tag{88}$$
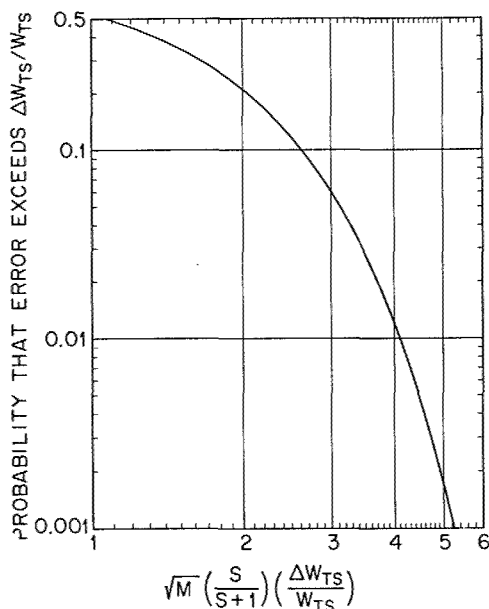
Fig. 3 - Probability of specified errors in Thomson-scatter signal-power measurement

Equation (89) is satisfied in this case if $\sqrt{M} \gg 1.3$.*

As this discussion shows, there may well be some practical applications for which values of M are used that do not satisfy this criterion. In such cases the more accurate expression, Eq. (84), must be used, but then no simple curve relating $\mathcal{P}$ and $\Delta w_{TS}/w_{TS}$ can be drawn. It becomes necessary to draw a family of curves with M as a parameter, or to select a specific value of $\mathcal{P}$ and for this value draw a curve for $[S/(S+1)] (\Delta w_{TS}/w_{TS})$ as a function of M. (Such curves would be analogous to those of Figs. 5 through 7, Part 1.) Table 7 shows how the values of $[S/(S+1)] (\Delta w_{TS}/w_{TS})$ vary with M for the particular case $\mathcal{P} = 0.001$. The last two columns show how the result of this exact computation compare with the approximate result that would be obtained from Fig. 3. That is, if the number in column 3 is called x, and the number in column 4 is y,

$$y = 100 \ (1 - 5.2514/x) \ . \tag{89}$$

As indicated, the approximate result is good enough for most purposes for $M \geq 1000$. The numbers in the third column are to be compared with the value 5.2514 obtained by the approximate method for this value of $\mathcal{P}$.

Table 8 relating $\mathcal{P}$ and k is useful for making calculations of this type. The values were machine computed from Eq. (82) for the specified values of $\mathcal{P}$ by an iterative method.

Measurement of Minimum Detectable Signal

Radar receivers are often tested by measuring the "minimum detectable signal," as a check on their level of performance. Actually a noise factor or noise temperature measurement is the best measure of receiver performance, but the minimum-signal measurement can be made somewhat more easily, and is thus a more practical method

---

*It is to be noted here that the test should be made in terms of $\sqrt{M}$, rather than in terms of M, to avoid confusion as to the meaning of the symbol $\gg$. For example, if $\sqrt{M} \gg 1.3$ is assumed to mean the same as $M \gg 1.3^2$, then if $\gg$ is taken to mean "two orders of magnitude" for the square-root form of the relationship, it should be interpreted as "four orders of magnitude" when applied to the second form.

Table 7
Variation of $[S/(S+1)](\Delta w_{TS}/w_{TS})$ With M for $\mathcal{P} = 0.001$

M	$\left(\dfrac{S}{S+1}\right)\left(\dfrac{\Delta w_{TS}}{w_{TS}}\right)$	Col. 2 $\times \sqrt{M}$	Error Using Fig. 3 (%)
10	2.3500	7.431	29
100	0.5941	5.941	12
1,000	0.1730	5.469	4.0
10,000	0.05320	5.320	1.3
100,000	0.01668	5.273	0.41
1,000,000	0.005258	5.258	0.13

Table 8
Relation of $\mathcal{P}$ and k

$\mathcal{P}$	k
0.001	3.2908
0.01	2.5758
0.1	1.6449
0.5	0.67449

of routine performance testing. In fact, if the measurement is made properly, it is in effect an indirect measurement of the noise factor. As it is usually carried out, however, it lacks the precision usually attained in a properly made noise-factor measurement. The lack of precision is associated with the subjective nature of the measurement — its dependence on the judgment and experience of the person who performs it and makes the decision as to what signal level is "just detectable."

Moreover, considerable confusion sometimes exists as to the value of minimum detectable signal that should be observed if the receiver is operating properly (i.e., if its noise factor is as good as it should be). The purpose of the following discussion is to derive the correct formula for computing this value.*

As can be deduced from Eqs. (8) and (9) of Part 1, the following equation relates the minimum detectable signal power (watts) and other parameters of the radar system:

$$P_{r(min)} = k\,T_s\,V_0\,C_B/\tau ,\qquad (90)$$

where $k = 1.38 \times 10^{-23}$ watt-sec/deg is Boltzmann's constant, V_0 is the visibility factor, C_B is the bandwidth correction factor (Eq. (17) and Fig. 1, Part 1), and τ is the radar pulse length in seconds.

The minimum-signal measurement is usually made with a signal generator connected to the receiver input. Therefore the system noise temperature is

---

*This section of the report is based on an informal paper written by the author in 1962 in the Search Radar Branch, Radar Division, NRL.

$$T_s = T_g + T_e ,$$ (91)

where T_g is the Kelvin temperature of the signal-generator output impedance, and T_e is the receiver noise temperature. T_e is related to the receiver noise factor F_n by Eq. (41), Part 1:

$$T_e = T_0(F_n - 1) ,$$ (92)

where T_0 is the IEEE reference temperature for noise-factor measurement, 290°K. If $T_g \approx T_0$, as is usually true, at least within the precision of other factors in the measurement, Eq. (91) becomes

$$T_s = F_n T_0 ,$$ (93)

and Eq. (90) becomes

$$P_{r(min)} = k F_n T_0 V_0 C_B/\tau .$$ (94)

It is customary to express $P_{r(min)}$ in decibels relative to 1 milliwatt. The equation in these terms, with τ expressed in microseconds and with the numerical values of k and T_0 inserted, is

$$P_{r(min)(dBm)} = -114 + V_{0(dB)} + C_{B(dB)} + F_{n(dB)} - 10 \log \tau_{\mu sec} .$$ (95)

For most well-designed radar systems, $C_B \approx 1$, or $C_{B(dB)} \approx 0$. The usual method of making the measurement is to connect the receiver output to an oscilloscope, corresponding to a radar A-scope display. A calibrated pulse signal generator is connected to the receiver input, with the pulse length and repetition frequency set to the appropriate values. The visibility factor to be used in Eq. (95) is then given by a curve of the type of Fig. 8, Part 1. As mentioned in the figure caption, this curve is for 0.5 probability of detection and for an unspecified false-alarm probability. A human observer performing a minimum-detectable-signal measurement seldom if ever attempts to evaluate these parameters. This is another reason for the relative imprecision of such measurements, compared to noise-factor measurement. Experience has shown that the typical observer probably evaluates $P_{r(min)}$ more nearly at the 0.9 probability level than at the 0.5 level. The 0.9 probability values are approximately 2 dB higher than the 0.5 values, for pulse repetition frequencies below about 1000. (At higher repetition frequencies the 0.9 and 0.5 probability curves gradually come together and tend asymptotically to approximately the constant value $V_{0(dB)} = -8$.)

A possible source of error in the measurement is the use of too low a sweep speed on the oscilloscope. As discussed in Part 1, a loss of signal detectability occurs if $s\tau < d$, where s is the sweep speed in millimeters per second, τ is the signal pulse length in seconds, and d is the cathode-ray-tube spot diameter in millimeters. Therefore, care should be taken to use an adequate sweep speed. Usually a value of $s\tau$ equal to or greater than 1 mm is sufficient.

Sometimes in measurement of $P_{r(min)}$ the receiver is left connected to the antenna, and the signal from the signal generator is fed in through a directional coupler. With this arrangement, the system noise temperature in Eq. (90) is given by the following equation, rather than by Eq. (91):

$$T_s = (T_a + T_r)/L_r + T_e .$$ (96)

In this equation T_a is given by Eq. (37) and T_r by Eq. (40) of Part 1. L_r is the receiving-transmission-line loss factor. Equation (96) is based on the assumption that the directional coupler is located at the receiver input. The attenuation of the coupler must of course be considered in evaluating the signal power at the receiver, but it does not affect the noise calculation if the coupling factor (signal attenuation) is large — e.g., 20 dB or greater. Evaluation of T_a and T_r is discussed in Part 1 and also later in this report. (Equation (36) of Part 1 would apply instead of Eq. (96) if the directional coupler were located at the antenna terminals instead of at the receiver terminals.) The equation corresponding to Eq. (95) for this situation is

$$P_{r(min)(dBm)} = -138.6 + V_{0(dB)} + C_{B(dB)} + 10 \log T_s - 10 \log \tau_{\mu sec} \ . \tag{97}$$

4. CALCULATION OF PROPAGATION FACTOR

In Part 1, a method of calculating the pattern-propagation factor F that results from sea-reflection interference when earth curvature is significant is described. This method is taken from Ref. 1. It is based on the use of parameters S and T, from which the factors J, K, and D are calculated. These factors are graphed in Fig. 17 of Part 1. The graphs were machine plotted from digital-computer solution of the appropriate equations. In this section the method of calculating these graphs will be described, and some additional topics relating to the pattern-propagation factor will be discussed.

Computer Solutions for J, K, and D

The basic equations for computing J, K, and D as functions of S and T are given in Ref. 1, Sec. 2.13, p. 113 ff. However, the solutions given there are not explicit. Therefore the equations on which the computer solutions were based, resulting in the graphs presented in Part 1, will be presented here briefly. The starting point is the assumption that the parameters S and T are given; they are calculated from Eqs. (57) and (58) of Part 1.

In each case, the calculation is done through intermediate variables S_1 and S_2, which are related to S and T by the equations

$$S = (S_1 + S_2 T)/(1 + T) \tag{98}$$

and

$$S_2(1 - S_1^2) = S_1 T(1 - S_2^2) \ . \tag{99}$$

Eq. (99) can be solved for S_2, giving

$$S_2 = \left[\sqrt{(1 - S_1^2)^2 + 4 S_1^2 T^2} + S_1^2 - 1 \right] / 2 S_1 T \ . \tag{100}$$

The equations for J, K, and D in terms of these quantities are

$$J = (1 - S_1^2)(1 - S_2^2) \ , \tag{101}$$

$$K = \frac{(1 - S_1^2) + T^2(1 - S_2^2)}{1 + T^2} \ , \tag{102}$$

and

$$D = \left[1 + \frac{4 S_1^2 S_2 T}{S(1 - S_1^2)(1 + T)}\right]^{-1/2} . \tag{103}$$

A suitable plotting procedure would be to start with arbitrarily chosen values of S_1 and T, calculate S_2 and S from Eq. (100) and (98), then find J, K, and D from Eqs. (101), (102), and (103). It was decided however, to plot contours of constant J and K. Therefore the procedure actually followed for J was to select arbitrary values of J and T, then to iterate Eq. (101) with respect to S_1, with the appropriate substitution for S_2 given by Eq. (100). In this way the required values of S_1 and S_2 (through Eq. (100) were found. Then S was found from Eq. (98). A similar procedure was followed for K.

A plot of D, however, was done differently, because it was decided that a more readable graph would result if D were plotted (on a logarithmic scale) as a function of S with T as a parameter. Therefore the procedure for each selected value of T was to go through a suitable range of values for S_1 to allow plotting the curve of D, finding the values of S from (in order of their use) Eqs. (100) and (98).

The plot of Fig. 18 of Part 1 was made by computing J and K as just described; D was also computed by the method described for J and K — that is, by the iterative method starting with the appropriate values of S and T. Then F was computed from (in order of their use) Eqs. (59), (60), (56), (62), and (61) of Part 1.

Plots of V and U for the Diffraction Region

The quantities V and U plotted in Fig. 19 of Part 1 are based on Figs. 2.19 and 2.20 of Ref. 1. The curves for V as a function of range X in natural units were computed from the basic equation (see Ref. 1, p. 122)

$$V_{dB} = 20 \log_{10}\left[2\sqrt{\pi X}\, e^{-2.02 X}\right] . \tag{104}$$

The curves for U were simply replotted from Fig. 2.20 of Ref. 1, since the computation is quite complicated; it is given by Eq. (428), p. 109, of Ref. 1.

The "Fine Lobe" Case

In Part 1, formulas were developed for calculating the pattern propagation factor F. An implicit assumption was made that the target moves sufficiently slowly in range to make this calculation meaningful. That is, it was assumed that if the radar scans in azimuth, the distance that the target moves in the time of one scan is such that F does not change greatly. In terms of lobe diagrams such as Figs. 14 and 18 of Part 1, it was assumed that the range change ΔR in the time of one scan is a small fraction of the range extent of a lobe.

If this assumption is not correct, then the calculation of F as described is not meaningful. If a plot of F as a function of range were made from experimental data under such circumstances, the result would not be a plot having the appearance of Fig. 18, Part 1. In effect, F behaves in this case like a randomly fluctuating quantity (stochastic variable). The blip-scan ratio ψ discussed in Part 1, and defined there by Eq. (86), is likewise a stochastic quantity rather than an analytic variable. The meaningful quantity is its

average value $\bar{\psi}$, which can be calculated, as shown by Alderson (9). The following derivation is excerpted from Alderson's report.

The general equation for F, for the sea-reflection-interference case, as given in Part 1, Eq. (61), can be written in the form

$$F(\xi) = \left| f(\theta) \sqrt{1 + x^2 + 2x \cos \xi} \right| , \tag{105}$$

where $f(\theta)$ is the antenna pattern factor, x is the magnitude of the "effective reflection coefficient," and ξ is the phase difference between the direct and reflected rays. As a target approaches in range R, ξ changes rapidly while θ and x change relatively slowly. Therefore, ψ can be found by averaging over ξ. The angle ξ is given by

$$\xi = \frac{4\pi h \sin \theta}{\lambda} J(S, T) + \phi , \tag{106}$$

in which J is the correction factor discussed earlier (Eq. 101), h is the radar antenna height, λ is the wavelength, θ is the target elevation angle, and ϕ is the phase angle of the sea reflection coefficient. (Since many of the equations of Part 1 are in terms of "mixed" systems of units, it should be noted that in this equation h, λ, and R must all be in the same units of length.) The correction factor J is equal to unity when earth curvature can be neglected.

The nature of the variation of ψ with range when F = 1 (free space) is due primarily to the target-cross-section fluctuation, which has been discussed in Part 1. The statistics of this fluctuation depend on the nature of the target. In the absence of specific target-fluctuation information, the Rayleigh probability-density function is the one that is usually assumed to apply to the signal voltage at the receiver.* The corresponding density function for the target cross section is given by Eq. (88), Part 1, and the blip-scan ratio is then given by Eq. (89), Part 1. Therefore, the average value of ψ, averaged over the full range of ξ (2π radians) is

$$\bar{\psi} = \frac{1}{2\pi} \int_0^{2\pi} 2^{-[R/R_{50} F(\xi)]^4} d\xi , \tag{107}$$

where R_{50} is the range at which $\psi = 0.5$ with F = 1 (free space). (This average is equivalent to averaging ψ over one full lobe of the interference pattern.) Alderson numerically

---

*The Rayleigh probability density function for a voltage v is

$$p(v) = 2 \ln(2)(v/v_{50}^2) 2^{-(v/v_{50})^2} ,$$

where v_{50} is the median value of the voltage. The more usual representation, which is entirely equivalent, is given by Eq. (77). This voltage density function corresponds to a target-cross-section fluctuation whose density function is

$$p(\sigma) = \frac{\ln 2}{\sigma_{50}} 2^{-\sigma/\sigma_{50}} .$$

This is a negative-exponential density function (not the Rayleigh function); but a target whose cross-section fluctuation is thus characterized is commonly called a "Rayleigh target," because of the resulting signal-voltage fluctuation.

integrated this equation to plot $\bar{\psi}$ as a function of R/R_{50}, for various values of the param-
eter x, Eq. (105). (Alderson equated this parameter to D, the divergence factor, as-
suming that ρ_0, r, and $f(\theta_2)/f(\theta_1)$ — see Eq. (62), Part 1 — were all equal to unity as is
often approximately true. Alderson's curves may be interpreted for the more general
situation by simply reading x in place of his D.) The resulting curves are shown as
Fig. 1 of Ref. 9. They show that for D = 0, corresponding to free space (no reflected
wave), the variation of $\bar{\psi}$ with range R is steeper than for nonzero values of D. In other
words, the additional signal fluctuation caused by a "fine lobe" structure results in lower
values of $\bar{\psi}$ at ranges appreciably less than R_{50}, and larger values of $\bar{\psi}$ at ranges
greater than R_{50}, compared to the free-space values. See Appendix (p. 47).

As noted in Part 1, these results are calculated without taking into account the addi-
tional fluctuation of the echo signals caused by the presence of noise in the receiving
system; the more exact analysis, including the effect of noise, has been made by Mallett
and Brennan (10). However, Alderson's results are valid when the minimum detectable
signal-to-noise ratio is relatively large (true when detection is based on observation of
a single pulse or integration of only a few pulses); moreover, the general conclusions
drawn from his curves are also valid in the more general case.*

Alderson (9) has applied this type of analysis to the problem of analyzing the effects
of ship pitch and roll on radar performance, as a function of the antenna vertical beam-
with in relation to the pitch and roll angles.

The Effect of Diffuse Forward Scattering

In Part 1, the reduction of the effective reflection coefficient caused by roughness of
the reflecting surface was discussed, and a formula (Eq. (56), Part 1) was given for com-
puting the ratio ρ/ρ_0, where ρ is the magnitude of the rough-surface reflection coeffi-
cient, and ρ_0 is the smooth-sea coefficient.

In this context, ρ may be called the *specular* reflection coefficient. Of the total
power incident upon a unit area of the sea surface, a fraction ρ^2 is specularly reflected
and another fraction $(1 - \rho_0^2)$ is transmitted through the surface and eventually absorbed.
The remaining fraction, equal to $\rho_0^2 - \rho^2$, is reflected *diffusely*. That is, there is no
coherent or analytical relationship of the phases of this portion of the reflected field at
points in space separated by appreciable distances. Moreover, in the case of the sea
surface, this phase relationship changes randomly with time.

The diffusely reflected field can thus be regarded as a randomly varying quantity in
both space and time. Its existence, however, means that the total field at any point in
space is really the vector sum of three components — the direct-path field, the specularly
reflected field, and the diffuse (randomly varying) field.

Because the diffusely reflected field can be regarded as the vector sum of reflections
from numerous independently related reflecting elements of the sea surface (11), the am-
plitude distribution of this field can be assumed to be Gaussian. It thus has a noiselike
character, and its combination at the receiver input with the direct-path and specularly-
reflected components will result, at the output of a linear detector, in a Rician distribu-
tion of signal amplitude (see Eq. (13)). The diffuse forward-scattered signal therefore

---

*Alderson notes that a procedure similar to his was described by T. E. Phipps and S. L. Waleszczak
in OEG (Chief of Naval Operations) Study 473, 29 May 1952 (Confidential). He also credits A. G.
Ferris, then of NRL, with the conception of Fig. 1, Ref. 9.

produces signal fluctuation, in addition to any fluctuation that may already be present from causes previously discussed.

The random field due to diffuse reflection will at some times and at some points in space add to the field resulting from interference of the direct and specularly reflected waves, and at other times and points it will subtract. On the average, however, since this field represents additional reflected energy, it will increase the field strength, and increase the probability of detection of a radar target. In the lobe maxima, where the specularly reflected signal is strongest, the relative effect of the diffuse reflection is least. Its effect increases as the ratio ρ/ρ_0 decreases — i.e., as the sea-wave height gets larger in relation to the product of the radar wavelength and the cosecant of the grazing angle.

However, it must not be supposed that the power ratio of the diffuse to the specular field *at a radar target* can be deduced from the ratio ρ/ρ_0 — that is, the power ratio at the target is not $\rho_0^2/\rho^2 - 1$, because, although this does represent the ratio of the diffusely to specularly reflected power per unit area of the sea, the diffusely reflected power is scattered in all directions while the specularly reflected power is concentrated in the forward direction. On the other hand, diffusely reflected signal power can reach the target from a wide area of the sea, if the radar beam is wide, while the specularly reflected signal is simply proportional to ρ^2 regardless of the radar beamwidth as long as it is not narrower (in the reflected-ray direction) than the angular width of the first Fresnel zone. Therefore the quantitative relationship of the diffuse and specular signal components is quite complicated.

The effect of the diffuse component will be most significant, of course, in the "nulls" of a smooth-sea interference pattern. Some further details of the effect are given by Blake (11) and subsequently by Beckmann and Spizzichino (12) and others. The effect is mentioned by Kerr (1), page 535.

5. PROPAGATION-MEDIUM LOSSES

Tropospheric Absorption

In Part 1, curves are given for the loss due to absorption of radar waves in the normal troposphere. Figure 21 gives the two-way (radar) absorption for total traversal of the troposphere; these results would apply, for example, for radar targets in outer space, such as satellites and other space objects. Since ionospheric absorption is not included, these curves apply fully only at frequencies at which ionospheric absorption is negligible — generally, above about 1000 MHz in the daytime, and above perhaps 500 MHz at night. At lower frequencies they apply for targets that are above the troposphere but below the ionosphere.

For radars used to detect aircraft and other targets in the troposphere, curves are needed which give the absorption as a function of range and angle. Such curves are presented in Part 1 as Fig. 22, with the radar frequency as a parameter. The method by which these curves were computed will now be described.*

---

*Some of this material was first presented by the author as a paper at the URSI-IRE meeting of Commission 2 at Washington, D.C., on May 6, 1959. This work was later described in an NRL Report (13) and in correspondence in IRE Transactions (14). The results there described were manually computed. Later they were programmed for computer solution and extended to higher frequencies; this work was described at the 1963 International Symposium of the IEEE Group on Antennas and Propagation at Boulder, Colorado. The description of these computations is presented here for the first time in report form.

Van Vleck's equations (15-17) for absorption per nautical mile* of oxygen, γ_1, and water vapor, γ_2, were written in the following form:

$$\gamma_1 = \frac{53.5\,p}{T^2\,\lambda^2}\left[\frac{h\,\alpha_1}{1/\lambda^2 + h^2\,\alpha_1^2} + \frac{h\,\alpha_1}{(2 - 1/\lambda)^2 + h^2\,\alpha_1^2}\right.$$

$$\left. + \frac{h\,\alpha_1}{(2 + 1/\lambda)^2 + h^2\,\alpha_1^2}\right] \tag{108}$$

and

$$\gamma_2 = \frac{8.5\times 10^4\,\rho}{T^{5/2}\,10^{278/T}\lambda^2}\left[\frac{h\,\alpha_2}{(0.7418 - 1/\lambda)^2 + h^2\,\alpha_2^2}\right.$$

$$\left. + \frac{h\,\alpha_2}{(0.7418 + 1/\lambda)^2 + h^2\,\alpha_2^2}\right] + \frac{6.3\,\rho\,h\,\alpha_3}{\lambda^2\,T} \ . \tag{109}$$

The symbols are defined as follows:

p - total atmospheric pressure, millibars

T - absolute atmospheric temperature, degrees Kelvin

λ - radio wavelength, centimeters

α_1 - line-breadth constant[†] for oxygen at sea level, taken to be $0.02\ cm^{-1}$

α_2 - line-breadth constant for water-vapor at sea level, applicable to the $\lambda = 1.348$ cm line ($f = 22.2$ GHz), taken to be $0.1\ cm^{-1}$

α_3 - an effective line-breadth constant for the residual absorption due to water-vapor lines in the infrared region, taken to be $0.27\ cm^{-1}$

h - a function expressing the dependence of the line-breadths on altitude (pressure and temperature)

ρ - water-vapor density, grams per cubic meter

The function h has been assumed, following Van Vleck, to be proportional to pressure and inversely proportional to the square root of the temperature. Therefore, with inclusion of a constant factor to give $h = 1$ at $T = 293°$ K and $p = 1013$ mb,

$$h = 1.7\times 10^{-2}\ p\,T^{-1/2}\ . \tag{110}$$

Experiments of Hill and Gordy (18) indicate that the dependence on temperature may actually be about $T^{-0.85}$ instead of $T^{-0.5}$. However, this would result in a maximum increase of γ of about 10 percent at the altitude of lowest atmospheric temperature, in the

*One international nautical mile equals 1.852 kilometers exactly.

†Following Van Vleck's practice the line-breadth constant is here expressed in terms of the wave-number breadth, which he denoted ($\Delta\nu/c$). The value 0.02 is equivalent to a frequency width of 600 MHz. This is the half-width of the absorption line at the half-maximum point.

30,000 to 80,000 foot region. The increase at 10,000 feet is about 3 percent, and of course there is no change at zero altitude where the absorption is greatest. Since the contribution to integrated path loss above 30,000 feet is a relatively small percentage of the total, the net effect of a change to the Hill-Gordy line-breadth temperature dependence would be small.

The values of γ_1 and γ_2, and the total $\gamma = \gamma_1 + \gamma_2$, were computed at altitude intervals of 1000 feet up to a 100,000-foot altitude, assuming the pressure and temperature values of the ICAO Standard Atmosphere (19) (essentially the same as the ARDC model atmosphere). A water-vapor density of 7.5 grams per cubic meter at zero altitude was assumed, and the height dependence was patterned after the average statistics for Washington, D.C., over a 10-year period (for which the zero-altitude average density was 6.18 grams per cubic meter (13)). These atmospheric models were entered into the computer as a table of values at 1000-foot altitude intervals.

The total path loss for two-way propagation (as for monostatic radar) was computed, for each of the specified elevation angles, by integrating 2γ as a function of distance from the antenna along the actual ray paths. The one-way loss (as for radio communication, telemetering, etc.) would be half the two-way decibel values. The range-height-angle relationship was computed on the basis of the CRPL Exponential Reference Atmosphere (20) (a model of the atmospheric refractivity profile), for a surface refractivity $N_s = 313$.

However, the values in the range 45 to 75 GHz are shown dotted in Fig. 21, Part 1, because the formulas used for calculating the absorption are not valid in the region of the oxygen resonance at 60 GHz. The "resonance" is actually a group of several closely-spaced lines, and the formula employed is the "centroid approximation" as given by Van Vleck (15), which is valid only to within about 15 GHz of the 60-GHz region. The approximate behavior in the 60-GHz region is shown dotted. The exact behavior has been calculated by Meeks and Lilley (21) (for oxygen in the absence of any water-vapor absorption) by summing the absorption due to each of the individual resonance lines.

As discussed in some detail by Straiton and Tolbert (22), questions exist concerning the exact validity of the Van-Vleck-Weisskopf (VVW) pressure-broadening formula (17) in the far wings (far from the resonances). The use of the value $\alpha_s = 0.27$, not justifiable theoretically, is an attempt to account empirically for observed deviations from theory of the residual contribution of the infrared lines to the water-vapor absorption, but the correction thus obtained is not fully satisfactory. Similarly, oxygen absorption "in the far wings" may be incorrect, as computed from the VVW formula. However, this is the best theory available at the present time, and there is considerable reason to believe that the results are not grossly incorrect.

The results are in good agreement, for the frequencies at which they made computations, with the curves published by Bean and Abbott (23) and by Hogg (24) for total transit of the troposphere. (Hogg's work was incidental to computations of tropospheric noise temperature, as discussed in Sec. 6 of this report.) To the author's knowledge, curves comparable to those of Fig. 22, Part 1, for the attenuation between points within the troposphere, have not been calculated elsewhere.

The curves thus computed for a standard atmosphere are of course subject to some variation in the actual atmosphere when the pressure, temperature, and water-vapor content differ from the standard values assumed. However, the ordinary variation of pressure and temperature will produce negligible variation of the oxygen absorption. Since this is the predominant absorption at the below about 1000 MHz, the results will not vary much below this frequency. From about 3000 MHz up to about 25 GHz, however, the water-vapor absorption is a significant part of the total absorption, and consequently

variations of the atmospheric water-vapor content will cause significant variations of the absorption. If it is desired to correct for this variation, it is necessary to plot separately the oxygen and water-vapor absorptions, instead of combining them as was done in the curves of Part 1. The two absorption components are directly additive. If the water-vapor component is plotted for a standard water-vapor density (e.g., 7.5 g/m³), the decibel absorption for other values of vapor density is simply proportional to the density. The extreme range of water-vapor density is from about 2 g/m³ (in the arctic) to about 20 g/m³ (in the tropics).

Ionospheric Absorption

In Part 1 the absorption that occurs in the ionosphere was discussed briefly, with reference to a paper by Millman (25). Some more recent work by Millman (26) provides additional information. In Part 1 the equation

$$L_{I(dB)} = A/f^2 \qquad\qquad (111)$$

was given for the ionospheric loss in decibels, and values of A were given for low-angle rays, high-angle rays, daytime, and nighttime, for frequency f in megahertz. Although not there specified, the low-angle figures were for rays of 10-degree initial elevation angle and the high-angle figures were for 90-degree initial angle. Eq. (111) is applicable to radar frequencies at and above 100 MHz, which includes the great majority of radars. The attenuation at 100 MHz is not great, and because of the inverse-square frequency relationship, ionospheric absorption is unimportant at frequencies higher than a few hundred megahertz.

Millman's more recent report contains curves (Fig. 35) from which values of A, Eq. (111), can be deduced as given in Table 9. These values (for 10- and 90-degree angles) are slightly different from those of Millman's earlier paper. It must be realized, however, that the values depend heavily on what characteristics of the ionosphere are assumed to be "standard." In addition to the pronounced diurnal variation indicated in Table 9, there are also lesser seasonal and solar-sunspot-cycle variations.

Table 9
Values of A for Eq. (111)

Elevation Angle (degrees)	A (dB)	
	Daytime	Nighttime
0	2.1×10^4	6.4×10^2
5	2.0×10^4	6.0×10^2
10	1.8×10^4	5.4×10^2
30	8.4×10^3	3.0×10^2
90	4.4×10^3	1.6×10^2

Absorption by Rain

For basic radar range calculation, no rainfall is assumed, since in most areas of the world rainfall is the exception rather than the rule. Nevertheless, rain does occur often enough to be a factor in assessing overall radar detection-range capability at

microwave frequencies. Absorption by rain is seldom important below about 10 GHz, however.

The computation of radar maximum range for a specified rainfall attenuation per unit distance and a specified range extent of the rainfall area has been discussed in Part 1 (Sec. 7). The problem faced by a radar designer, or specification writer, is to specify the characteristics of a standard rainfall in which the radar must meet a specified detection-range capability. This is a problem that would best be handled by a meteorologist; but to the author's knowledge, no standards of this type have been proposed. Therefore, the following proposals are made for use by radar designers and specification writers until more authoritative standards become available.

A light rain (27) is considered to be one of about 1 mm/hr (0.04 in/hr). Such rains can extend over wide geographical areas, and to altitudes of about 10,000 ft (23). Although the rainfall rate may be anything but uniform within the geographical and altitude extent of the rain, for the purpose of defining a convention (see Part 1, Sec. 1) for absorption by rain it is not unreasonable to assume a uniform rate. Therefore it is proposed that a "standard light rain" (for computing radar performance) be defined as one with a rate of 1 mm/hr (0.04 in/hr) extending over an indefinitely large geographical area and to 10,000-ft altitude.

A heavy rain (27) is one of about 16 mm/hr (0.64 in/hr). However, such rains are usually limited in their geographical extent, seldom exceeding a diameter of about 20 miles. Their altitude extent, however, may be 20,000 ft or greater. A proposed standard heavy rain is therefore one of 16 mm/hr covering a 20-nautical-mile diameter geographically, and extending to 20,000-ft altitude.

An intense rain, of the type observed in severe thunderstorms, is one of about 50 mm/hr (2 in/hr) or greater. Rates of up to 100 mm/hr or more are not uncommon, but these are usually very local and of short duration in nontropical regions. The altitude of a thunderstorm may be 40,000 ft or greater. A standard intense rain will therefore be arbitrarily defined as one of 50-mm/hr rate, 2-nautical-mile diameter, and 40,000-ft-altitude extent.

It is to be emphasized that these proposed conventions by no means represent or even bracket all possible rainfall conditions. Possibly the most characteristic feature of rain is its great variability, both in space and time. The assumption of uniform rain rate within an appreciable volume of space is physically unrealistic; but, for computing absorption such an assumption is justified since the total path attenuation is proportional to the average absorption over the path.

The attenuation produced by rain of specified intensity is given theoretically by J.W. Ryde (28,29). A comparison of Ryde's theory with numerious experimental results has been made by Medhurst (30). (Medhurst also applied machine computation to Ryde's equations, thus refining the basis for comparison of theory and experiment.) He found that the agreement is not quantitatively good, but there is qualitative agreement. The experimental attenuations are often greater than those predicted theoretically. This may be partly explained by inadequacies of the experimental techniques. Medhurst suggests a number of possible theoretical factors not considered by Ryde's theory which may also partially explain the discrepancies. Semplak and Turrin have made an additional suggestion (31).

Despite this disagreement, the Ryde theory is probably adequate for computing expected attenuation for the rainfall conventions proposed here, since they are only very approximately related to reality in any specific case. Medhurst has computed values of the theoretical attenuation for a number of frequencies as a function of the precipitation

rate. His results are plotted in Fig. 4 for the rainfall rates of the proposed conventions and a temperature of 20 °C. Temperature affects the attenuation in a very complicated way. Medhurst (30) has published a table of temperature correction factors based on the theory of Ryde.
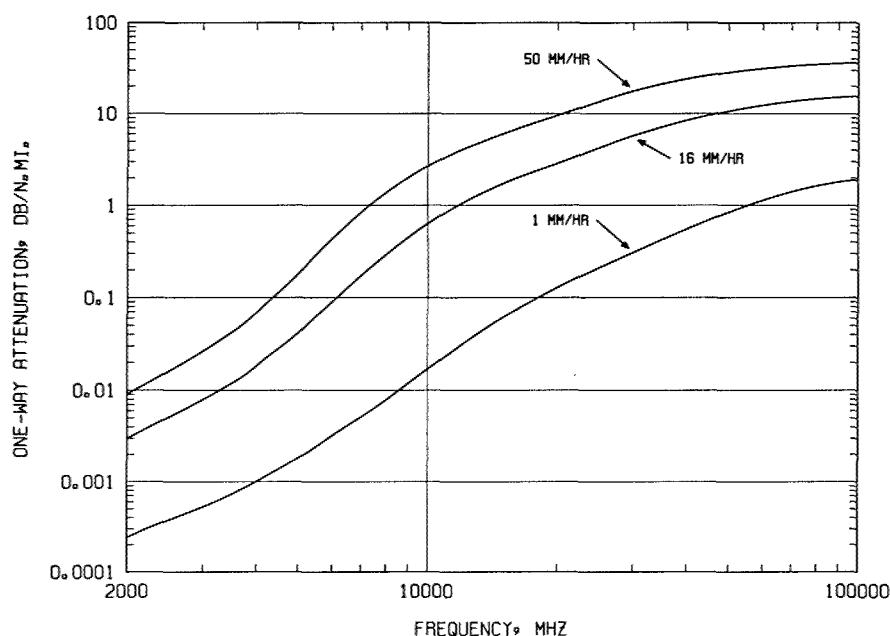

Fig. 4 – Attenuation by rain of specified rates,
after Medhurst (30)

An excellent discussion of rain attenuation (and also of radar echoes from rain) is contained in Ref. 1, Chapters 7 and 8. Although it was written three decades ago, this book is still a most valuable source of information on these subjects. Absorption and radar reflection by hail, snow, and fog or clouds are also discussed. Much useful meteorological information and radar theory are also given by Battan (32).

6. NOISE TEMPERATURE CALCULATION

System Noise Temperature

The objective of noise temperature calculation is to obtain a measure of the noise power level at the output of the system. This in turn permits computation of the output signal-to-noise ratio, which is the principal factor that determines the system sensitivity. It is not, however, the sole factor if the term signal-to-noise ratio is interpreted to mean the "instantaneous" (or single-pulse) signal-to-noise ratio. The ultimate sensitivity is then also affected by signal-processing procedures such as integration or averaging. (These two terms are virtually synonymous.) Here the term signal-to-noise ratio will be meant in the instantaneous or preprocessing sense.

The concept of system noise temperature and its relationship to the noise temperatures of the system components have been treated in some detail in Part 1, for the case

of a "single response" system; multiple-response systems present special problems which are discussed in Refs. 33 and 34.*

Most radar receiving systems are of the single-response type, although occasionally, at the very highest microwave frequencies, a superheterodyne receiver without preselection may be used. Such a receiver has two input response frequencies — the desired signal frequency, and the image frequency (the difference and the sum of the local oscillator and intermediate frequencies). For the appropriate method of calculating the system noise temperature in this case, Ref. 34 should be consulted; additional details will be found in Ref. 33.

The definitions of Ref. 34 do not contain the term "system noise temperature." It is used here because it has become established by wide usage among radio and radar engineers; it is a *de facto* standard term. The equivalent term used in Ref. 34 is "operating noise temperature (of a system)," designated T_{op}.

If a receiving system consists of a cascade of twoport transducers, it is in principle possible to dissect it at any junction of two of the system elements, and then to regard the portion at the input end as a "source," and the remaining portion as "the receiver." The "system" then has two elements, and the following equation of Ref. 34 applies:

$$T_{op} = T_i + T_e , \tag{112}$$

where T_i is the noise temperature of the source (called the "input termination" in Ref. 34), and T_e is the effective input noise temperature of the receiver. The latter quantity is related to the receiver noise factor F_n by the equation

$$T_e = (F_n - 1) T_0 , \tag{113}$$

where by IEEE standards $T_0 = 290°K$.

In this type of procedure, the dissection is essentially arbitrary. For example, if the actual system consists of *three* cascaded components, as shown in Fig. 5, it could be dissected either at the receiver terminals J_2 (Case 1) or at the antenna terminals J_1 (Case 2). In the former case, the transmission line (which generates noise because of its loss factor L_r and nonzero thermal temperature (T_t) is regarded as a part of the antenna, and the intrinsic antenna noise temperature T_a is modified by the effect of the line loss. In the latter case, the receiver noise temperature is modified by the line loss. In either case, the output signal-to-noise ratio can be correctly computed, but the value of T_{op} obtained in the two cases will be different. Since this point sometimes causes considerable confusion, it will be discussed here in some detail. The notation T_{op} (operating noise temperature) will, however, now be replaced by the more commonly used T_s (system noise temperature).

The noise temperature T_i in Eq. (112) multiplied by Boltzmann's constant $k = 1.38 \times 10^{-23}$ (watt-sec/°K) and by the noise bandwidth of the system B_n gives the available output noise power of the input termination — i.e., the noise power that would be delivered to a matched load of bandwidth B_n connected at the output terminals of the source.[†] When

---

*The problem of multiple-response systems is considered in appreciably greater detail in Ref. 33 than in the IEEE Standard and tutorial paper, Ref. 34. However, the definitions used in Ref. 33, which was written before the IEEE Standard was issued, do not conform exactly to the IEEE Standard definitions. Since definitions are basically arbitrary, the treatment in Ref. 33 is valid and useful in terms of its own definitions, but it differs in some details from the treatment of Ref. 34.

†This formula is actually an approximation, analogous to the Rayleigh-Jeans approximation of Planck's radiation law. The more exact expression is $hfB_n/(e^{hf/kT} - 1)$, where h is Planck's constant and f is frequency, Hz. The approximation is invalid if $f/T > 4 \times 10^8$.
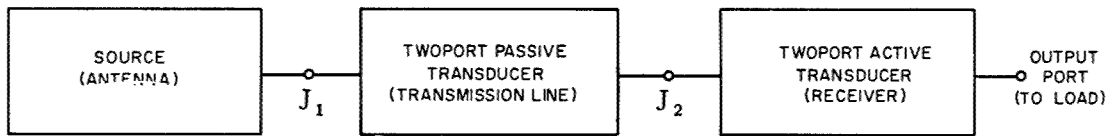
Fig. 5 – A three-component cascade receiving system

the system is dissected at the antenna terminals (Case 2) it is evident that the correct value for T_i is thus simply T_a, the antenna noise temperature.

If the dissection is at the receiver terminals (Case 1), however, the value of T_i reflects the resultant available noise power (at the receiver terminals) of both the antenna and the transmission line. As has been discussed in Part 1, the available output noise power in bandwidth B_n of a passive twoport transducer (e.g., transmission line) of available loss factor L_r and thermal temperature T_t is

$$P_o = kT_t(1 - 1/L_r) B_n \cdot \tag{114}$$

This figure assumes that an input termination (e.g., antenna) is connected to the transmission-line input terminals, but it does not include the noise power at the receiver terminals due to the antenna. This contribution is directly additive to the transmission-line noise power, as mentioned in Part 1, because the two noise sources are not coherent (phase correlated). The antenna noise power at this point is

$$P_{o(ant)} = kT_a B_n/L_r \cdot \tag{115}$$

The divisor L_r expresses the fact that the antenna noise is attenuated by the transmission line. The total noise is therefore

$$k T_i' B_n = kB_n [T_a/L_r + T_t(1 - 1/L_r)] \cdot \tag{116}$$

The term on the right in brackets is evidently equal to T_i'. (The "prime" on T_i is here used to express the fact that it is not the same as T_i when the system is dissected at the antenna terminals.) The total system noise temperature for Case 1 then becomes

$$T_{s(1)} = T_a/L_r + T_t(1 - 1/L_r) + T_e \tag{117}$$

(by substituting the solution for T_i' in Eq. (116) for T_i in Eq. (112).)

For Case 2, T_i is simply T_a, but T_e (which will now be denoted T_e') must express the combined effect of the transmission line and the receiver. The principle invoked to solve this problem is that the product $k T_e' B_n G$ must represent the contribution of the transmission-line-and-receiver combination to the total system output noise power, where G is the overall power gain of the combination. It is evident that this overall gain is G_r/L_r where G_r is the receiver gain and L_r is the transmission-line loss factor. Therefore the equation that must hold is

$$k T_e' B_n G_r/L_r = P_{o(line)} + P_{o(receiver)} \tag{118}$$

where P_o denotes noise power at the receiver *output* terminals. From Eq. (114) it is evident that

$$P_{o(line)} \approx k\, T_t (1 - 1/L_r)\, B_n\, G_r \qquad (119)$$

and it is obvious that

$$P_{o(receiver)} = k\, T_e'\, B_n\, G_r \; . \qquad (120)$$

By substituting Eqs. (119) and (120) into Eq. (118) it is found that

$$T_e' = T_t(L_r - 1) + L_r\, T_e \; . \qquad (121)$$

Hence the total system noise temperature for Case 2 is

$$T_{s(2)} = T_a + T_t(L_r - 1) + L_r\, T_e \; . \qquad (122)$$

Comparing this result with Eq. (117), it is readily seen that

$$T_{s(2)} = L_r\, T_{s(1)} \; . \qquad (123)$$

It will now be shown that either Eq. (117) or (123) can be used to calculate the system signal-to-noise ratio correctly. Suppose that a signal power $P_{s(ant)}$ is available at the output terminals of the antenna. The signal power at the system output will be

$$P_{s(out)} = P_{s(ant)}\, G_r / L_r \; . \qquad (124)$$

In Case 1 the noise power output is given by

$$P_{n(out)} = k\, T_{s(1)}\, B_n\, G_r \qquad (125)$$

and in Case 2 it is given by

$$P_{n(out)} = k\, T_{s(2)}\, B_n\, G_r / L_r \; . \qquad (126)$$

But since $T_{s(2)} = L_r\, T_{s(1)}$ by Eq. (123), these two values of $P_{n(out)}$ are identical, and the signal-to-noise ratio $P_{s(out)}/P_{n(out)}$ is therefore the same in both cases, as was to be proved.

Thus it makes no difference which dissection point is chosen, except for the following consideration. In calculating radar maximum range, the system loss factor L must contain as one of its factors the receiving line loss factor L_r if the Case 1 representation of T_s is used. If the Case 2 representation is used, however, in effect there is no receiving line loss (i.e., $L_r = 1$), because the receiving line is considered *to be a part of the receiver;* its noise is incorporated into the computation of the effective noise temperature of the receiver, and its loss factor L_r reduces the effective receiver gain.

The Case 1 representation was employed in the first edition (1962) of Part 1 of this report, and L_r was included in the computation of L. In the second edition (1969), the Case 2 representation is used, and the factor L_r is not included in computation of L. As the foregoing discussion implies, either method results in the same calculated range.

The fact is, of course, that in a system consisting of a multiplicity of cascaded units, the dissection of the system can be made at any junction of two system components, and in this way many possible values of the system noise temperature can be obtained, all valid, and all applicable to one and the same system. In each such case, however, the receiving line loss factor L_r must be evaluated differently; it must represent only those losses that occur prior to the "dissection" point.

This matter is discussed in some detail in Ref. 33, in terms of what is there called the *referral principle*. The system noise temperature is said to be *referred* to the point in the system which, in the foregoing discussion, is called the dissection point. Very general equations are there presented for the system noise temperature — i.e., for the temperature of a system of n cascaded components with the system noise temperature referred to the junction of the mth and (m + 1)th components of the system (m < n).

In 1962 there seemed to be historical precedents for taking the receiver input terminals as the system-noise-temperature reference point. However, in the 1962 edition of Part 1 of this report, the concept of the system *input* noise temperature was also discussed. At that time, the author also chose to define *antenna* noise temperature in terms of the noise power captured from space by the antenna aperture prior to its reduction by any ohmic losses in the antenna; this decision was made in the absence of any IEEE standard definition of antenna noise temperature. Subsequently (35) an IEEE standard definition has been adopted; it defines the antenna noise temperature in terms of the noise power available at the actual terminals of the antenna. As discussed in Part 1, this noise is a composite of noise received from external radiating sources and noise generated in dissipative portions of the antenna.

Since 1962 there has been a trend toward defining the system noise temperature with the antenna terminals as the reference point. Therefore this practice has been followed in the second edition of Part 1, in terms of the IEEE definition of the antenna noise temperature.

For the special case of this reference point, the general equation for the system noise temperature of a single-response cascade system of N twoport transducers (not including the antenna, which is regarded as the input termination of the first transducer) becomes

$$T_s = T_a + \sum_{i=1}^{N} T_{e(i)}/G_i , \qquad\qquad (127)$$

which was given in Part 1 as Eq. (35). In this equation $T_{e(i)}$ is the effective input noise temperature of the ith transducer and G_i is the available gain of the system between its input terminals (antenna terminals) and the *input* terminals of the ith transducer. As noted in Part 1, by this definition $G_1 = 1$ always. For the three-component (two-transducer) system that has been analyzed here, $G_2 = 1/L_r$, $T_{e(1)} = T_t(L_r - 1)$, and $T_{e(2)} = T_e$, where T_e without additional subscripts denotes the receiver noise temperature as defined by Eq. (113)). Thus Eq. (127) becomes Eq. (122). For further details and explanations, see Ref. 33.

Antenna Noise Temperature

As discussed under the preceding heading, the IEEE standard definition of antenna noise temperature defines it to be the composite result of noise from external radiating sources and noise from the internal dissipative parts of the antenna. In Part 1, curves are presented (Fig. 11) which give the noise temperature of a typical radar antenna due to external radiating sources, for conventional assumptions concerning the external environment, and omitting the contribution of radiation from the ground (earth). The text of Part 1 explains how the value of T_a obtained from these curves is modified to take into account the ground radiation and the effect of antenna dissipative losses. The purpose of this discussion will be to explain in some detail how the curves of Fig. 11, Part 1, were calculated.

As there explained, these curves represent the composite effect of (i) galactic noise, (ii) sun noise, (iii) tropospheric noise, and (iv) cosmic blackbody radiation. These contributing sources are in general functions of the radar frequency and the antenna beam pointing direction. To plot curves that can be used as conventions for radar range calculation, the variation of galactic noise with galactic coordinates is ignored, and a mean value is assumed (actually the geometric mean of maximum and minimum values). The variation of tropospheric noise with antenna beam elevation angle is taken into account, so that a family of curves with beam elevation angle as the family parameter results. The sun is assumed to be in the visible sky, but not in the main beam of the antenna pattern; a conventional value of sidelobe level in the sun direction is assumed (unity-gain or 0-dB side lobes). The cosmic blackbody radiation is assumed to be independent of both frequency and direction and to be of noise temperature 2.7°K (36). This small contribution to the total antenna temperature is of little importance ordinarily, but it may be of significance for antennas of the ultralow-noise variety (37). (The value 3.5°K was originally estimated for this temperature, but the value most recently reported is 2.7°K.)

The well-known basic equation for the noise temperature of an antenna is

$$T_a = \frac{1}{4\pi} \int_0^{2\pi} \int_0^{\pi} T(\theta,\phi) \, G(\theta,\phi) \, \sin\theta \, d\theta d\phi \, , \tag{128}$$

in which $T(\theta,\phi)$ is the noise temperature "seen" by the antenna in the direction (θ,ϕ), and $G(\theta,\phi)$ is the antenna gain in that direction. Since $T(\theta,\phi)$ is seldom known in sufficient detail to permit this integration to be carried out exactly, it is usual to average $T(\theta,\phi)$ over finite segments of solid angle. If the entire 4π steradians is thus subdivided into n segments, Eq. (128) becomes

$$T_a = \sum_{i=1}^{n} T_{a(i)} \, , \tag{129}$$

where $T_{a(i)}$ is the average noise temperature within the ith solid-angle segment, whose solid-angular size will be denoted Ω_i. A general formula for $T_{a(i)}$ is

$$T_{a(i)} = \frac{\Omega_i \, \bar{G}_i \, \bar{T}_i}{4\pi} = \alpha_i \bar{T}_i \, , \tag{130}$$

where $\bar{G}_i$ and $\bar{T}_i$ are the average values of $G(\theta,\phi)$ and $T(\theta,\phi)$ within Ω_i. The fraction $\alpha_i = \Omega_i \, G_i/4\pi$ can be interpreted, in terms of a transmitting antenna, as the fraction of the total power radiated into the solid angle Ω_i.

At some frequencies the noise temperature in a particular direction is partially due to astronomical sources (the galaxy and the sun) and partly due to radiation by the lossy atmosphere. In such cases the net temperature is the noise temperature of the distant source reduced by the loss factor of the atmosphere and augmented by the atmospheric radiation. For example, in the case of the galactic noise the formula is

$$T_{a(gal)} = \alpha_{gal} \left(\frac{\bar{T}_{gal}}{L_{atm}} + T_{atm} \right) \, , \tag{131}$$

where $T_{a(gal)}$ is the contribution of the galactic solid angle to the total antenna temperature, α_{gal} is defined by Eq. (130), $\bar{T}_{gal}$ is the average galactic noise temperature before

attenuation by the atmosphere, and T_{atm} is the atmospheric noise temperature. A similar procedure is followed for the sun noise contribution.

As explained above, the ground noise contribution was assumed to be zero in plotting Fig. 11 of Part 1. The procedure there described for adding a ground noise contribution simply corresponds to adding a term $\alpha_G T_G$ in Eq. (129), where α_G represents the fraction of 4π steradians subtended by the ground as viewed by the antenna multiplied by the average gain of the side lobes that view the ground, and T_G is the noise temperature of the ground.

If the ground is completely absorbing, its noise temperature is equal to its thermal temperature, T_{tG} (Kelvin). If it is completely reflecting, its noise temperature is determined by its reflection of the galactic noise, sun noise, etc. In general, its emissivity is $\mathscr{E} = 1 - \mathscr{R}$, where $\mathscr{R}$ is its reflectivity,* or the fraction of incident power that is reflected. In these terms,

$$T_G = \mathscr{E} T_{tG} . \tag{132}$$

The galactic noise is assumed to follow the frequency law $f^{-2.5}$ (38, 39), and its noise temperature at 100 MHz is taken to be 3050°K. This is the geometric mean of the maximum and minimum values reported by Brown and Hazard (40), which at 100 MHz are 18,650°K and 500°K. The geometric mean was taken so as not to give undue weight to galactic "hot spots" of small angular dimensions. Also, this procedure causes the mean to fall halfway between the maximum and minimum values (dashed lines) on the logarithmic temperature scale of Fig. 11, Part 1. The formula thus obtained for the galactic noise contribution to the antenna temperature is

$$T_{a(gal)} = \alpha_{gal} T_{100} (100/f_{MHz})^{2.5} / L_{atm} , \tag{133}$$

where T_{100} is the galactic temperature at 100 MHz, f_{MHz} is the frequency in megahertz, α_{gal} is given by Eq. (130), and L_{atm} is the atmospheric loss factor (a function of elevation angle).

The value assumed for α_{gal} in computing the curves of Fig. 11, Part 1, is unity, because these curves are for an ideal antenna which has no side or back lobes that view the ground. Correction factors to be applied for actual antennas are discussed in Part 1. A typical value of α_{gal} for a real antenna is about 0.85.

The noise temperature of the quiet sun, T_{sun}, was taken from a curve published by Kuiper (41), after Smerd (42). The values in the range of frequencies plotted in Fig. 11, Part 1, are given in Fig. 6. The sun noise contribution to the antenna temperature was then calculated from Eq. (130) with α_{sun} (= $\Omega_{sun} \bar{G}/4\pi$) equal to 4.75×10^{-6}, with $\bar{G} = 1$. The sun's visible (optical) diameter subtends an angle of 1/2 degree as seen from the earth, and this value of α_{sun} corresponds to this diameter. The value $\bar{G} = 1$ means that the sun was assumed to be viewed in a unity-gain (0-dB) side lobe of the antenna pattern. It was also assumed that the sun was in an active state, so that its noise temperature was ten times the quiet level. Consequently, the formula for the sun noise contribution to total antenna temperature is

---

*It is to be noted that the reflectivity $\mathscr{R}$ is not the same as the specular reflection coefficient ρ discussed in Part 1, Sec. 6. Where ρ is the ratio of the specularly reflected field strength (e.g., volts per meter) to the incident field strength, $\mathscr{R}$ is the ratio of the total power (e.g., watts) reflected from a unit area of surface, including both specular and diffuse reflection, to the power incident on the area.

Fig. 6 – Calculated apparent noise temperature of the quiet sun, after Smerd (42). A coronal temperature of 10^6 degrees and a chromospheric temperature of 10^4 degrees Kelvin were assumed. Dots represent observational data taken during the period 1942-1950.
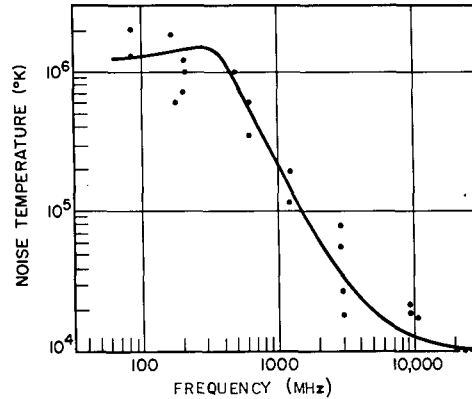
$$T_{a(sun)} = 4.75 \times 10^{-5} \, T_{sun}/L_{atm} \, . \tag{134}$$

Although the sun's optical diameter is 1/2 degree, its "noise diameter" is considerably greater at the lower end of the radar frequency spectrum, because the corona is there the principal source of radiation, while at the upper end of the spectrum the radiation comes from the chromosphere. This increase of effective diameter at the lower frequencies is taken into account by the method of calculating T_{sun} (41).

The atmospheric loss factors are obtainable from Fig. 21 of Part 1. Since the values shown there are decibel values for two-way transit of the troposphere, the relation between the atmospheric loss factor L_{atm} in Eqs. (131), (133), and (134) and the decibel (dB) values of Fig. 21, Part 1, is

$$L_{atm} = 10^{dB/20} \, . \tag{135}$$

The noise temperature of the atmosphere T_{atm} is given (43) by the equation

$$T_{atm} = 0.2303 \int_0^\infty \gamma \, T_{t(atm)} \, e^{-0.2303 \int_0^R \gamma(r) \, dr} \, dR \, , \tag{136}$$

in which the variable of integration R is distance along the ray path from the antenna, $\gamma(R)$ is the attenuation in decibels per unit distance along the path, and $T_{t(atm)}$ is the thermal temperature of the atmosphere. (The numerical factor 0.2303 occurs in this equation because γ is defined to be in decibels rather than nepers per unit distance.) The values of γ were computed as described in Sec. 5, and the $T_{t(atm)}$ values used were those of the ICAO Standard Atmosphere (19).

These results were applied to Eq. (129) to compute antenna noise temperature as a function of frequency from 100 MHz to 100 GHz, for seven elevation angles. The computations were done by the NRL CDC-3800 computer from a FORTRAN program (TAPLOT) written by the author, and machine plotted by the NRL Gerber Model 875 Automatic Drafting Machine from punched paper tape obtained from the computer results. The resulting plot is Fig. 11 of Part 1. In the left part of the figure the dashed lines represent maximum and minimum values of the galactic and solar noise temperatures, and in the right part they represent maximum (low-angle) and minimum (high-angle) tropospheric noise. The maximum curve assumes a sun noise temperature 100 times the quiet level of Fig. 6, while the minimum curve assumes zero sun noise (nighttime radar operation). The slight

spreading of the solid curves in the UHF region is due to the variation of absorption of galactic noise by atmospheric loss (see Eq. (131)), causing a higher antenna temperature at higher elevation angles. That is, the reduction of the galactic noise at the low angles caused by atmospheric absorption is greater than the attendant tropospheric noise radiation, in this frequency region. The peculiar bump in the curves at about 500 MHz is due to the knee of the sun noise curve at about that frequency (Fig. 6).

Transmission-Line Noise Temperature

In Part 1, Sec. 5, the formula

$$P_{no} = k T_t B_n (1 - 1/L) \tag{137}$$

was given for the noise power output in a bandwidth B_n of a twoport passive transducer (e.g., transmission line) whose thermal temperature is T_t and whose loss factor is L. This results in the formula

$$T_r = T_t (L - 1) \tag{138}$$

for the *input* noise temperature of the transducer. Eq. (137) was derived by Dicke (43) in the following manner.

The derivation will be made in terms of Fig. 5, in which all components are assumed to be linear and passive. Initially it is assumed that the source is at thermal temperature T_t, and the other two components are at zero temperature, so that they generate no noise power. In that case, the available noise power at J_1 is $k T_t B_n$ (in accordance with Nyquist's Theorem), and that at J_2 is $k T_t B_n /L$, where L is the loss factor (available loss) of the twoport transducer. It is not important for this derivation that if the transducer were at zero temperature its dissipative loss would be zero. In fact, L is the *available* loss, which is the product of the mismatch loss at J_1 and the dissipative loss, if any, in the transducer. But the argument being given is a primarily logical rather than a purely physical one, and it is permissible here to assume that the loss factor is independent of the temperature.

If now the temperature of the twoport transducer is raised to the temperature T_t, all other temperatures remaining unchanged, the available power at J_2 will be $k T_t B_n$, again by Nyquist's Theorem. Since the contribution of the source to the power at J_2 must be the same as before, the contribution of the twoport transducer must be the difference between the available power at J_2 before and after the temperature was raised. This difference is

$$P_{no} = k T_t B_n - k T_t B_n /L = k T_t B_n (1 - 1/L) , \tag{139}$$

as was to be proved.

This result was derived by assuming that the source and the transducer are brought to the same thermal temperature. However, because the system is linear and the noise voltages in the source and transducer are noncoherent, it is evident that the noise contribution of the transducer to the total noise at J_2 is not dependent on the temperature of the source. Consequently the result deduced by assuming a special temperature for the source is actually a general result.

Further details of this matter and other matters discussed in this section will be found in Ref. 33.

7. DERIVATION OF FORMULA FOR RANGE PREDICTION ERROR

In Part 1, Eq. (92) is presented without proof. It expresses the range prediction error, or standard deviation, as a function of the standard deviations of the factors in the range equation. This equation was derived in 1961 by John Wood, then of the NRL Radar Division Mathematics Staff, in response to a request by the author to S. F. George, Head of the Mathematics Staff. Wood's derivation is presented here. The starting point was the following radar range equation, which was given in Part 1:

$$R = k \left[\frac{P_t^{1/4} \tau^{1/4} G_t^{1/4} G_r^{1/4} \sigma^{1/4} F}{f^{1/2} T_s^{1/4} V_0^{1/4} L^{1/4}} \right] \tag{140}$$

The symbols are defined as follows:

k - a constant depending on the units used

P_t - transmitter pulse power

τ - pulse length

G_t - transmitting antenna gain

G_r - receiving antenna gain

σ - target cross section

F - pattern-propagation factor

f - radar frequency

T_s - system noise temperature

V_0 - visibility factor (minimum-detectable signal-to-noise power ratio)

L - system loss factor.

The problem as presented was to find the standard deviation of R, given the individual standard deviations of the parameters on the right-hand side of Eq. (139). The right-hand side contains the product (and quotient) of terms. Convenient theorems exist concerning the standard deviation of the sum (and difference) of terms. The suggestion was therefore made, in presenting the problem to Wood, that it would be tractable in terms of a logarithmic formulation. This approach was followed.

The following theorems are employed. Given a function $f(x_1, x_2, \ldots, x_n)$, it is known that

$$(\delta f)^2 = \sum_{i=1}^{n} \left(\frac{\partial f}{\partial x_i} \right)^2 (\delta x_i)^2 . \tag{141}$$

For the case when

$$f(x_1, x_2, \ldots x_n) = y_1(x_1) \, y_2(x_2) \cdots y_n(x_n) \tag{142}$$

the corresponding logarithmic relationship is

$$\log f = \sum_{i=1}^{n} \log y_i(x_i) \quad . \tag{143}$$

Differentiating,

$$\frac{\partial \log f}{\partial x_j} = \frac{1}{f} \frac{\partial f}{\partial x_j} = \frac{1}{y_j} \frac{\partial y_j}{\partial x_j} \quad , \tag{144}$$

and Eq. (141) therefore gives

$$\frac{(\delta f)^2}{f^2} = \sum_{i-1}^{n} \frac{1}{y_i^2} \left(\frac{\partial y_i}{\partial x_i} \right)^2 (\delta x_i)^2 \quad . \tag{145}$$

The left-hand side of this equation is the square of the fractional error in f. Applying the right-hand side of Eq. (144) to Eq. (140) gives

$$\frac{1}{R} \frac{\partial R}{\partial P_t} = \frac{1}{P_t^{1/4}} \frac{1}{4} P_t^{-3/4} = \frac{1}{4P_t} \quad . \tag{146}$$

This shows that an expression can be obtained for the fractional error of R in terms of the fractional errors of the other parameters. The result is

$$\left(\frac{\delta R}{R} \right)^2 = \left(\frac{1}{4} \frac{\delta P_t}{P_t} \right)^2 + \left(\frac{1}{4} \frac{\delta \tau}{\tau} \right)^2 + \left(\frac{1}{4} \frac{\delta G_t}{G_t} \right)^2 + \left(\frac{1}{4} \frac{\delta G_r}{G_r} \right)^2 + \left(\frac{1}{4} \frac{\delta \sigma}{\sigma} \right)^2$$

$$+ \left(\frac{\delta F}{F} \right)^2 + \left(\frac{1}{2} \frac{\delta f}{f} \right)^2 + \left(\frac{1}{4} \frac{\delta T_s}{T_s} \right)^2 + \left(\frac{1}{4} \frac{\delta V_0}{V_0} \right)^2 + \left(\frac{1}{4} \frac{\delta L}{L} \right)^2 \quad . \tag{147}$$

This result is equivalent to Eq. (92), Part 1.

Appendix

GRAPH FOR PREDICTING THE EFFECT OF A
FINE-LOBE INTERFERENCE PATTERN

The graph shown below is a reproduction of Fig. 1 of Ref. 9, which is discussed in Sec. 4 of this report. It is reproduced here because Ref. 9 is no longer readily available.
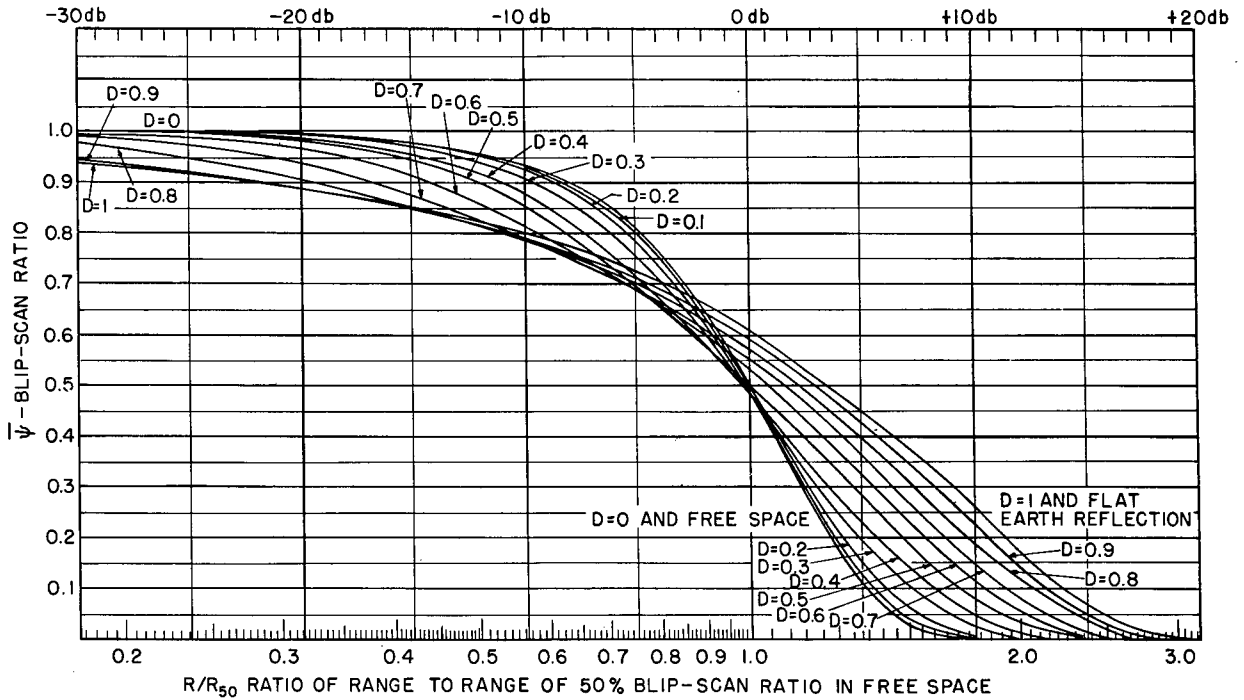

Fig. 1 – The blip-scan ratio, averaged over one lobe of the interference pattern, as a function of the normalized range. R_{50}, the free-space range for a 50-percent blip-scan ratio on a given target, is equal to $R_0 \sqrt[4]{\sigma_{50}}$, where σ_{50} is the median cross section of the target and R_0 the free-space range on a one-square-meter nonscintillating target. D is divergence factor.

REFERENCES

1. Kerr, D.E., (ed.), "Propagation of Short Radio Waves," Volume 13 of MIT Radiation Laboratory Series, McGraw-Hill, New York, 1951

2. North, D.O., "An Analysis of the Factors Which Determine Signal/Noise Discrimination in Pulsed-Carrier Systems," Proc. IEEE 51 (No. 7), 1016-1027, July 1963 (originally published as RCA Laboratories Report PTR-6C, June 1943)

3. Rice, S.O., "Mathematical Analysis of Random Noise," Bell System Tech. J. 23 No. 4), 282-332 (July 1944) and 24 (No. 1), 46-156 (Jan. 1945)

4. Robertson, G.H., "Operating Characteristics for a Linear Detector of CW Signals in Narrow-Band Gaussian Noise," Bell System Tech. J. 46 (No. 4), 755-774 (Apr. 1967)

5. Fehlner, L.F., "Marcum and Swerling's Data on Target Detection by a Pulsed Radar," Johns Hopkins University Applied Physics Laboratory Report TG-451, July 1962, and Supplement, TG-451A, Sept. 1964

6. Marcum, J.I., "A Statistical Theory of Target Detection by Pulsed Radar," and "Mathematical Appendix," Trans. IRE IT-6 (No. 2), 59-267 (Apr. 1960) (originally published as Rand Corporation Research Memoranda RM-754, Dec. 1947, and RM-753, July 1948)

7. Swerling, P., "Probability of Detection for Fluctuating Targets," IRE Trans. IT-6 (No. 2), 269-308 (Apr. 1960) (originally published as Rand Corporation Research Memorandum RM-1217, Mar. 1954)

8. Blake, L.V., et al., "A VHF-UHF Missile- and Space-Research Radar with a 150-Foot Steerable Antenna," NRL Report 5801, Aug. 1962

9. Alderson, W.S., "Calculation of Radar Performance and the Effect of Roll and Pitch," NRL Report 4584, Aug. 1955 (DDC Accession No. AD 75708)

10. Mallett, J.D., and Brennan, L.E., "Cumulative Probability of Detection for Targets Approaching a Uniformly Scanning Search Radar," Proc. IRE 51 (No. 4), 596-601 (Apr. 1963)

11. Blake, L.V., "Reflection of Radio Waves from a Rough Sea," Proc. IRE 38 (No. 3), 301-304 (Mar. 1950)

12. Beckmann, P., and Spizzichino, A., "The Scattering of Electromagnetic Waves from Rough Surfaces," Pergamon, New York, 1963

13. Blake, L.V., "Curves of Atmospheric-Absorption Loss for Use in Radar Range Calculation," NRL Report 5601, Mar. 23, 1961

14. Blake, L.V., "Tropospheric Absorption Loss and Noise Temperature in the Frequency Range 100-10,000 Mc," IRE Trans. Antennas and Propagation (Correspondence) AP-10, 101 (Jan. 1962)

15. Van Vleck, J.H., "The Absorption of Microwaves by Oxygen," Phys. Rev. 71 (No. 7), 413-424 (Apr. 1, 1947)

16. Van Vleck, J.H., "The Absorption of Microwaves by Uncondensed Water Vapor," Phys. Rev. 71 (No. 7), 425-433 (Apr. 1, 1947)

17. Van Vleck, J.H., and Weisskopf, V.F., "On the Shape of Collision-Broadened Lines," Rev. Mod. Phys. 17 (Nos. 2 and 3), 227-236 (Apr. and July 1945)

18. Hill, R.M., and Gordy, W., "Zeeman Effect and Line Breadth Studies of the Microwave Lines of Oxygen," Phys. Ref. 93, 1019-22 (Mar. 1, 1954)

19. Minzner, R.A., et al., "U.S. Extension to the ICAO Standard Atmosphere," U.S. Weather Bureau and AFCRC, U.S. Govt. Printing Office, Oct. 1959

20. Bean, B.R., and Thayer, G.D., "CRPL Exponential Reference Atmosphere," NBS Monograph 4, U.S. Govt. Printing Office, Oct. 1959

21. Meeks, M.L., and Lilley, A.E., "The Microwave Spectrum of Oxygen in the Earth's Atmosphere," J. Geophys. Res. 68, 1683-1703 (Mar. 15, 1963)

22. Straiton, A.W., and Tolbert, C.W., "Anomalies in the Absorption of Radio Waves by Atmospheric Gases," Proc. IRE 48, 898-903 (May 1960); also, Tolbert, C.W., and Straiton, A.W., "Synopsis of Attenuation and Emission Investigations of 58 to 62 kMc Frequencies in the Earth's Atmosphere," Proc. IEEE 51, 1754-1760 (Dec. 1963)

23. Bean, B.R., and Abbott, R., "Oxygen and Water Vapor Absorption of Radio Waves in the Atmosphere," Geofisica Pura E Applicata (Milano) 37, 127-144 (1957)

24. Hogg, D.C., "Effective Antenna Temperature Due to Oxygen and Water Vapor in the Atmosphere," J. Appl. Phys. 30, 1417-1419 (Sept. 1959)

25. Millman, G.H., "Atmospheric Effects on VHF and UHF Propagation," Proc. IRE 46 (No. 8), 1492-1501 (Aug. 1948)

26. Millman, G.H., "A Survey of Tropospheric, Ionospheric, and Extraterrestrial Effects on Radio Propagation Between the Earth and Space Vehicles," General Electric Co. (HMED, Syracuse, N.Y.) Report TIS-R66EMH1, Jan. 1966

27. Humphreys, W.J., "Physics of the Air," 3rd ed, McGraw-Hill, New York, 1940

28. Ryde, J.W., "Echo Intensities and Attenuation Due to Clouds, Rain, Hail, Sand and Dust Storms at Centimetre Wavelengths," Report 7831, General Electric Co. Research Labs, Wembley England, Oct. 1941

29. Ryde, J.W., and Ryde, D., "Attenuation of Centimetre Waves by Rain, Hail, and Clouds," Report 8516, Aug. 1944, and Report 8670, May 1945, General Electric Co. Research Labs, Wembley, England

30. Medhurst, R.G., "Rainfall Attenuation of Centimeter Waves: Comparison of Theory and Measurement," IEEE Trans. Antennas and Propagation AP-13, 550-564 (July 1965)

31. Semplak, R.A., and Turrin, R.H., "Some Measurements of Attenuation by Rainfall at 18.5 GHz," Bell System Tech. J. 48, 1767-1787 (July-Aug. 1969)

32. Battan, L.J., "Radar Meteorology," University of Chicago Press, Chicago, Ill., 1959

33. Blake, L.V., "Antenna and Receiving-System Noise-Temperature Calculation," NRL Report 5668, Sept. 1961; available from the Clearinghouse for Scientific and Technical Information, 5285 Royal Rd., Springfield, Va. 22151 (Accession No. AD 265 414). Also summarized in correspondence (same title), Proc. IEEE 49 (No. 10), 1568-1569 (Oct. 1961)

34. IRE Standard 62 IRE 7.S2, and accompanying tutorial paper by H. A. Haus et al., "Description of the Noise Performance of Amplifiers and Receiving Systems," Proc. IRE 51 (No. 3), 434-442 (Mar. 1963)

35. IEEE Standard 149, "IEEE Test Procedure for Antennas," Jan. 1965, available from IEEE Headquarters, New York; also published in IEEE Trans. AP-13 (No. 3) 437-466 (May 1965)

36. Partridge, R.B., "The Primeval Fireball Today," Amer. Scientist 57 (No. 1), 37-74 (Spring 1969 issue)

37. Blake, L.V., "Low-Noise Receiving Antennas," Microwaves 5 (No. 3), 18-27 (Mar. 1966)

38. Ko, H.C., "The Distribution of Cosmic Radio Background Radiation," Proc. IRE 46 (No. 1) 208 (Jan. 1948)

39. Kraus, J.D., and Ko, H.C., "Celestial Radio Radiation," Ohio State University Report 1 of R.F. Project 673, AF Contract 19(604)-1591, May 1957; ASTIA No. 117-273

40. Brown, R.H., and Hazard, C., "A Model of the Radio-Frequency Radiation from the Galaxy," Phil. Mag. 44, 939 (Sept. 1953)

41. Kuiper, G.P., ed., "The Solar System; Vol. 1, The Sun," Univ. of Chicago Press, Chicago, 1953; Ch. 7, p. 485, Fig. 11

42. Smerd, S.F., "Radio-Frequency Radiation from the Quiet Sun," Australian J. Scientific Res. Series A, 3, 34 (1950)

43. Dicke, R.H., et al., "Atmospheric Absorption Measurements with a Microwave Radiometer," Phys. Rev. 70, 340-348 (Sept. 1946)

DOCUMENT CONTROL DATA - R & D

(Security classification of title, body of abstract and indexing annotation must be entered when the overall report is classified)

1. ORIGINATING ACTIVITY *(Corporate author)*	2a. REPORT SECURITY CLASSIFICATION
Naval Research Laboratory Washington, D.C. 20390	Unclassified
	2b. GROUP

3. REPORT TITLE

A GUIDE TO BASIC PULSE-RADAR MAXIMUM-RANGE CALCULATION, PART 2 — DERIVATIONS OF EQUATIONS, BASES OF GRAPHS, AND ADDITIONAL EXPLANATIONS

4. DESCRIPTIVE NOTES *(Type of report and inclusive dates)*

An interim report on the problem.

5. AUTHOR(S) *(First name, middle initial, last name)*

Lamont V. Blake

6. REPORT DATE	7a. TOTAL NO. OF PAGES	7b. NO. OF REFS
December 31, 1970	54	43

8a. CONTRACT OR GRANT NO.	9a. ORIGINATOR'S REPORT NUMBER(S)
NRL Problem 53R02-55.101	
b. PROJECT NO. RF05-151-402-4011	NRL Report 7010
c.	9b. OTHER REPORT NO(S) *(Any other numbers that may be assigned this report)*
d.	

10. DISTRIBUTION STATEMENT

Distribution of this document is unlimited.

11. SUPPLEMENTARY NOTES	12. SPONSORING MILITARY ACTIVITY
This is Part 2 of a previous report of the same title, NRL Report 6930	Department of the Navy (Office of Naval Research), Washington, D.C. 20360

13. ABSTRACT

    A previous report, designated Part 1, with the same main title, presented information of a practical nature, with little or no proofs, derivations of equations, or explanations, except that sources of information not originated by the author were cited, if previously published. This report, Part 2, presents the proofs, derivations, and explanations omitted in Part 1, together with some results which were either previously unpublished or are now out of print. The basic topics covered are probability of detection of a radar signal, calculation of the radar pattern-propagation factor, atmospheric losses, antenna noise temperature, and the relationship of range-prediction errors to the individual errors in the range-equation factors.

14. KEY WORDS	LINK A		LINK B		LINK C	
	ROLE	WT	ROLE	WT	ROLE	WT
Radar						
Pulse						
Range						
Detection						
Propagation, radio wave						
Probability of detection						
Signal detection						

DD FORM 1 NOV 65 **1473** (BACK)

(PAGE 2)

52